

Crystal Chemistry at High Pressure

Katerina P. Hilleke¹ and Eva Zurek^{1*}

¹Department of Chemistry, State University of New York at Buffalo, 777 Natural Sciences Complex, Buffalo, 14260-3000, NY, USA.

*Corresponding author(s). E-mail(s): ezurek@buffalo.edu;

Contributing authors: khilleke@gmail.com;

1 Introduction

Jupiter, the largest planet in our solar system, is a gas giant comprised mostly of hydrogen and helium. After penetrating its atmosphere, a mixture of hydrogen and helium, methane and ammonia, one would find a massive sea of hydrogen – behaving very differently than one might expect from general chemistry classes [1]. The hydrogen layer surrounding Jupiter’s core, under immense pressure and at high temperature, is metallic. This is just one example of how the pressure variable is so important in determining chemical and physical behavior, bearing consequences for the evolution and dynamics of planetary interiors [2].

Under pressure, the behavior of the elements as well as the compounds they form can change drastically from what we, as beings living and learning at 1 atmosphere, are used to. Hydrogen, as described above, can become metallic at high pressure, joining its Group I cousins the alkali metals. It may be perplexing then to learn that the alkali metals lithium [3] and sodium [4, 5] become semiconducting and insulating, respectively, when squeezed. Potassium starts to behave more like a transition metal [6–8]. When combined with one another, the unexpected behavior of the elements under pressure makes for correspondingly curious compounds. Sodium chlorides with vastly divergent stoichiometries from the typical 1:1 (Figure 1) have been predicted and synthesized [9], stubbornly inert helium atoms form a compound with sodium [10], and metal superhydrides wherein the hydrogen atoms coalesce into clathrate-like networks have been reported [11]. Various “rules” for the behavior of materials at high pressure have been proposed by Prewitt and Downs [12],

Grochala and co-workers [13], and Zhang *et. al.* [14], to name a few – and have undergone progressive revision as more is uncovered about the structures and materials far below us in the Earth’s core and far away in the planets and stars.

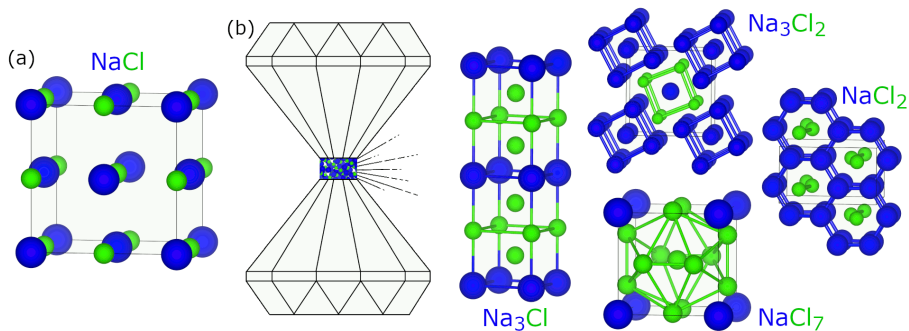


Fig. 1 The familiar crystal structure of NaCl, table salt, (a) is the only known stable compound of sodium and chlorine at ambient pressure. Under pressures exerted by a diamond anvil cell (b), a variety of additional stoichiometries and crystal structures decorate the sodium-chlorine phase diagram, including the $P4/mmm$ Na₃Cl, $P4/m$ Na₃Cl₂, $Imma$ NaCl₂, and $Pm\bar{3}$ NaCl₇ [10] structures shown here.

Over the past century, experimental methods have evolved to create progressively higher pressures in a laboratory setting, allowing us to directly probe the behavior of materials under extreme conditions. Pressures in the megabar range can now be routinely achieved, albeit still requiring delicate setups [15–17]. Diamond anvil cells (DACs) combine the superior hardness of this desired polymorph of carbon with its optical transparency, enabling the creation of the highest static pressures and interrogation of the sample via visual and spectroscopic means. Engineering advances from multistage compression apparatuses [18, 19] to toroidal DACs [20, 21] have driven the experimental ceiling for static pressures ever higher. Dynamic compression experiments under ramp or shock conditions, driven by gas guns, laser pulses, or magnetic fields can reach well into the terapascal regime [22–24], allowing us to study the behavior of diamond at 5 TPa [25] and iron at conditions thought to be in super-Earths [26]. Diagnostic techniques for characterizing the resulting substances can be difficult to implement in both dynamic and static compression, often requiring theoretical support for their interpretation [27].

Far cheaper than high-pressure experiments are computations modeling high-pressure systems. Band structures, phonons, Raman or infra-red spectra and numerous material properties can all be calculated without so much as stepping foot into a laboratory. Crystal structure prediction (CSP) techniques, not weighted down by preconceived, atmospheric pressure-based, notions of how atoms might appropriately arrange themselves in a unit cell, can identify which structures can exist under high-pressure conditions [28–30]. The computational exploration of potential energy landscapes will not be discussed

in our contribution; to learn about methods that can be employed to identify the global, as well as important local, minima we point the reader to an excellent chapter in this book “Crystal Structure Prediction” by Andreas Hermann, Lewis J. Conway and Chris J. Pickard. Exploratory calculations highlight promising phases for further experimental investigation, but computation can just as well follow experimental results, elucidating behavior and filling in the gaps. The resulting feedback loop of experiment and theory has driven the discovery and characterization of a plethora of phases ranging from the superhard [31–33] to the superconducting [11, 34–38].

In the following sections we build a framework for understanding the behavior of materials at high pressure, starting from the effects of pressure on the atoms themselves, driving electronic transitions and altering periodic trends. From there, the various manifestations of high pressure in the solid state are sorted into categories (which are not mutually exclusive, but rather illustrative), starting with exotic electronic structures and electrides. We discuss compounds of the noble gases and those containing elements that are immiscible at ambient pressure, as well as crystal lattices that contain bizarre geometrical motifs and bonding configurations. Finally, we survey the effects of high pressure on superconductivity, a field that has recently undergone a veritable explosion as high pressure phases toe the line of room-temperature superconductivity [39].

2 The atom under pressure

Chemistry describes the interactions between the 118 distinct elements that are organized in the periodic table, proposed by Mendeleev while classifying elements according to their chemical properties observed at atmospheric conditions. The trends found within the periodic table can be used to compare atoms according to their size, the number of electrons surrounding their nuclei, and to make predictions as to whether those electrons are held tightly or loosely. Moreover, the periodic table allows students and researchers to predict how different elements will interact with one another: will they form compounds, emulsions or alloys, or will they be unreactive? If reactivity is suspected, the periodic table can be used to guess if the bonds are covalent, ionic, or (usually) somewhere in between. Across the periodic table, trends in properties such as atomic radii, electronegativity, and oxidation state can be mapped, leading one to conclude that fluorine, the most electronegative element, will gain electrons in a binary phase thereby achieving an F^- configuration with a filled valence shell. On the other hand, cesium, as the least electronegative element (neglecting francium, whose miniscule half-life renders it basically experimentally irrelevant), typically assumes an oxidation state of 0 or +1.¹ Yet at high pressure, several Li_nCs phases have been predicted [44] where Cs attains unusual formal oxidation states thought to be in excess of -2 due to

¹When dissolved in amines or ethers, Na, K, Rb, and Cs can assume the unusual oxidation state of -1. [40] These so-called *alkalides* are thought to form ion-pairs with solvated metal cations. [41–43]

substantial electron transfer from lithium to cesium. How can the stability of these unintuitive stoichiometries and their resulting electronic structures be rationalized?

Let us consider electronegativity a little more. Although Pauling's [45] is the most widely adopted, a number of metrics have been used to produce scales of electronegativity for the elements. In Pauling's formulation, electronegativity differences between pairs of atoms A and B are calculated from the homo- and heteronuclear bond dissociation energies, then referenced against the electronegativity of H being set to 2.1 (later adjusted to 2.2). In this regime, the electronegativities of fluorine, lithium, and cesium are 3.98, 0.98, and 0.79, respectively. Several other scales have been proposed, including Mulliken's "absolute electronegativity" [46] being the average of the first ionization energy and electron affinity of an atom [47]. Dong *et al.* modify the Mulliken definition for elements under high pressure taking as a reference the homogeneous electron gas rather than the vacuum [48]. Allen's electronegativities are derived from the average energies of the valence electrons in the atom [49], and a closely related scheme has recently been proposed by Rahm *et al.* [50–52], where electronegativity is calculated as the average of the electron binding energies of ground state valence electrons – approximately translated to the Allen scale if averaging over valence electrons alone. Broadly speaking, the common factor of importance in all of these is the collection of atomic orbital energies and the differences between them. Under pressure, those change.

The prototypical model for understanding the quantized behavior of energy levels in a confined system is the particle in a box. The resulting energy levels for a particle of mass m in a box of width L are given by $E_n = \frac{\hbar^2 n^2 \pi^2}{2mL^2}$, where n is the principal quantum number. To consider the effects of pressure on this model, we could simply make the box smaller by reducing the width L , which has the effect of increasing the E_n . Thus, energy levels (orbital energies) will increase under pressure. The complicating factor is that the rate of this increase is not the same for each orbital because the number of radial nodes plays a role. The peak density of a 4s orbital is further from the nucleus than a 4p orbital, since the electrons occupying the 4s orbital must maintain orthogonality to those in the 1s, 2s, and 3s orbitals, while those in the 4p orbital must only contend with the 3p and 2p orbitals (this analogy may be extended to the 4d and 4f shells). With more electron density being further from the nucleus, the electrons in the 4s orbital will feel the effects of pressure more strongly than those in the 4p orbital. This is illustrated schematically in Figure 2a and 2b. At certain levels of confinement, electronic $ns \rightarrow np$, $ns \rightarrow (n-1)d$, and $(n-1)d \rightarrow (n-2)f$ transitions can become favorable. This is the reason why pressure drives rearrangements of the orbital energies of an atom, with ensuing electronic transitions. (In section 3.2, we will explore the opportunities presented by another sort of destination orbital, this time one not centered on an atom.)

In compressed lithium, the ground state electronic configuration transitions from $1s^2 2s^1 \rightarrow 1s^2 2p^1$, while cesium undergoes a $6s^1 \rightarrow 5d^1$ pressure induced

transformation. The exact pressures at which these electronic changes occur depend, of course, on the chemical environment of the lithium or cesium atoms – and in calculations, on the theoretical methodology. In Cs, the $s \rightarrow d$ transition is thought to drive the transformation to the complex Cs-III structure with 84 atoms in the unit cell that is stable near 4.2 GPa [53–58], while in lithium the pressure at which the s - p mixing occurs is believed to be somewhat higher, in the megabar to multimegabar range, dependent on the chemical environment and level of theory [57, 59–61]. Another example includes potassium, whose complex phase diagram under pressure (see, *e.g.* Figure 2c,d), has been in part attributed to this $s \rightarrow d$ electronic transition. [62] The energies of core orbitals can also become relevant; for example, in Cs-VI the 5p bands hybridize with the 6s [63, 64], making them accessible for chemical interactions, and the core orbitals of K have also been proposed to be key to its structural diversity. [62] Overall, one effect of pressure on the alkali metals is that their electronegativities undergo quite a rearrangement, ending up with cesium being more electronegative than lithium [48, 57]. From this perspective, the formation of cesium anions in the Li_nCs phases begins to make sense.

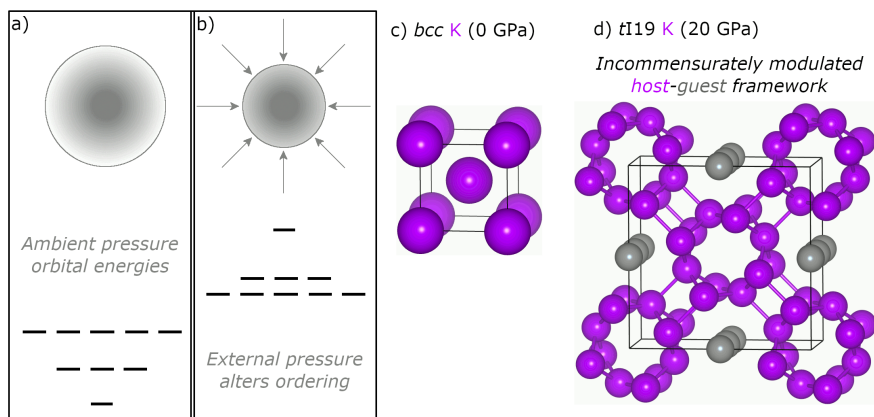


Fig. 2 External pressure on an atom raises the energy of atomic orbitals as they are constrained to a smaller space, but the rate of this increase differs between s , p , and d orbitals (a), (b), favoring $s \rightarrow d$ transitions for many of the alkali metals, including potassium. Potassium adopts the *bcc* structure at 0 GPa (c) but at higher pressures takes on a series of complex structures including the incommensurately modulated host-guest *tI19* phase [65] (d).

Among the d -block similar reorderings are predicted to take place, with the group 10 metals Ni, Pd, and Pt preferring d^{10} closed-shell configurations, as compared to the s^2d^8 favored at ambient conditions, while the group 11 and 12 metals become electron donors [48]. The former transition is associated with a spike in the estimated chemical hardness – obtained as half of the HOMO-LUMO gap – of Ni, Pd, and Pt, reaching values comparable to some of the noble gases. This is contrary to the general trend where the hardness of

most of the elements in the periodic table decreases with pressure as energy levels become closer to one another [48]. The resulting changes in the relative hardness of pairs of elements can lead to changes in compound stability arising from HSAB (hard-soft acid-base) arguments, and the appearance of strange multicenter bonding manifolds in certain high pressure phases have been linked to general increases in softness [66].

From transition-metal-like behavior in the s -block to relative inertness in the formerly- d^8 -transition metals, atoms under compression can behave very differently from their ambient-pressure selves, and the consequences for materials under pressure are far-reaching. We will now explore some of the wild and wonderful structures and phenomena that result.

3 The crystal under pressure

At ambient pressure a majority of the solid, metallic elements of the periodic table adopt very simple, symmetric, structures that are close-packed. The most stable geometries are those that minimize the free energy. However, at low temperatures the entropic contributions between different solid phases are typically negligible, so computational studies often employ the enthalpy to determine the structures that are preferred. With increasing pressure the enthalpy, consisting of the internal energy and pressure-volume terms ($H = U + PV$), becomes dominated by the PV term. It would be natural, therefore, to imagine that close-packed structures with increased coordination numbers become preferred at high pressures. The reality, however, does not coincide with our expectations. For example, within cesium the nearest neighbor coordination number first increases from 8 (bcc) to 12 (fcc), then decreases to about 10 (Cs-III), 8 (Cs-IV) and finally increases again to 10/11 (Cs-V) and 12 (Cs-VI). These structural transitions are believed to be driven by the previously discussed pressure-induced $s \rightarrow d$ valence electronic transition within the constituent atoms, which causes the interatomic distances to become smaller compared to the ranges of the wavefunction [53].

Moving beyond elemental crystal structures, several compounds with seemingly bizarre stoichiometries (at least from the perspective of minds that experience a 1 atmosphere reality) have been predicted and/or synthesized under pressure. The familiar combination of sodium and chlorine, table salt and prototypical ionic compound with a 1:1 ratio, is not the only stable crystalline structure in the Na-Cl phase diagram. At least two unique stoichiometries, Na_3Cl and NaCl_3 , were synthesized, and several others were predicted to become stable when squeezed [9]. Noble gases xenon, argon, and helium are active components of solid compounds that have been synthesized [10, 67, 68], and *very* hydrogen-rich compounds such as YH_9 , LaH_{10} , and CaH_6 that are high-temperature superconductors with superconducting critical temperatures (T_c s) approaching room temperature have been made [11, 37, 69–72]. These metal superhydrides are materials-by-design success stories inspired by theoretical predictions [34, 35, 73].

In the following sections, we explore the plethora of exciting materials that can be created using high pressure, with all their intriguing structural and behavioral phenomena. While their stability and existence can be traced to the pressure driven electronic rearrangements of the constituent atoms described in Section 2, the manifestations of these rearrangements can take many forms. Below, we describe a variety of illustrative phases sorted into a series of categories, but by necessity these categories will, at times, overlap. Nevertheless, all exemplify the ramifications of high pressure on solid-state chemistry.

3.1 Electronic structure

At atmospheric pressure, the stoichiometries of many inorganic solid-state compounds can be predicted from the most common oxidation states of their constituent elements. Usually, alkali metals and alkaline earth metals possess oxidation states of +1 and +2 respectively, so when combined with the O^{2-} ion one would expect Na_2O and MgO , as well as K_2O and SrO to form. The noble gases are mostly inert, the p-block is amenable to forming covalently bonded networks, and while a wide variety of oxidation states, which correspond to various filled or half-filled orbitals, are available to several transition metals, Zn, Cd, and Hg steadily persist in maintaining their d^{10} configurations.

The consequences of the orbital energy shifts discussed in Section 2 mean that several of these “rules” no longer apply at high pressures, and elements can adopt unusual oxidation states in compounds with unexpected stoichiometries. The Li_nCs phases [44] used to illustrate the effects of pressure on electronegativity provide one such example. Above 70 GPa, the very lithium rich Li_5Cs phase is predicted to become stable, joined at higher pressures by Li_3Cs , Li_4Cs , and $LiCs$ [44]. Remarkably, the calculated Bader charges on the Cs atoms in these stoichiometries are all more negative than -1, and since calculated Bader charges frequently underestimate formal oxidation states, in these compounds Cs may attain a formal oxidation state that is potentially lower than -2. While alkali metal anions (alkalides) have previously been captured at ambient pressures with cryptands [74], they achieve charges only up to -1 with the additional electron going into the ns orbital. In the case of the Li_nCs phases, however, pressure induces significant $Li\ 2s \rightarrow 2p$ and $Cs\ 6s \rightarrow 5d$ electronic transitions, with the latter increasing progressively with higher Li content, thereby facilitating the acceptance of electron density by the typically unoccupied Cs 5d orbitals.

For K, Cs, and Rb the pressure-driven $ns \rightarrow (n - 1)d$ transitions led to predictions of transition-metal like behavior [6, 75] in the formation of intermetallic compounds with actual transition metals [8, 76–78]. Within some of these compounds, the transition metal elements assume exotic electronic configurations, as in the case of the predicted potassium iridide K_3Ir (Figure 3a) containing the Ir^{3-} anion [79]. The Ir 5d orbital becomes fully occupied as a result of electron transfer from K, echoed in the later predicted Rb_3Ir and Cs_3Ir phases [80]. K_3Ir and Rb_3Ir share the $Pmnm$ Cu_3Ti structure type, while

Cs_3Ir adopts the $P2_1/m$ Ni_3Ta type, which consist of $\text{Ir}@M_8$ and $\text{M}@M_8$ distorted cubes, and $\text{Ir}@M_{12}$ distorted cuboctahedra respectively. In combination with Li under high pressure, Au displays a similar ability to adopt a significantly negative formal charge of less than -3 in the predicted phases Li_4Au and Li_5Au – where electrons donated from Li are placed into the empty Au 6p orbitals [81], which are less destabilized than the Li 2s or 2p under pressure.

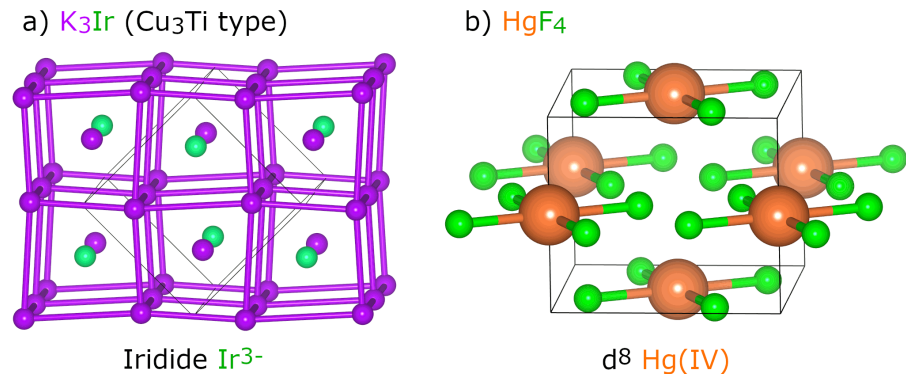


Fig. 3 High pressure compounds where the transition metal atoms adopt curious electronic configurations in (a) K_3Ir [79] (Cu_3Ti type), with $\text{Ir}@M_8$ and $\text{K}@M_8$ distorted cubes and iridide Ir^{3-} anions, and (b) HgF_4 [82], in which d^8 configurations on the Hg lead to square planar geometries.

Pressure can also promote chemical interactions with core or semi-core orbitals, as in the case of HgF_3 and HgF_4 [82]. These stoichiometries are predicted to become stable above 73 and 38 GPa, respectively, and above 200 GPa HgF_4 is computed to decompose into HgF_3 and F_2 . The $I4m$ symmetry HgF_4 crystal possesses square planar HgF_4 units typical of a d^8 organometallic complex, with the Electron Localization Function (ELF) [83] confirming covalent Hg-F interactions. To form the four Hg-F bonds, not only the Hg 6s but also two of the semicore 5d electrons are required. In HgF_3 , the $Fm\bar{3}m$ structure (which distorts below 100 GPa to $C2/m$ symmetry) involves a fluorite-type HgF_2^+ lattice stuffed with F^- ions, leaving Hg with a d^9 configuration. A series of predicted CsF_n phases, in which the Cs 5p electrons participate in Cs-F covalent bonds, are another example of the pressure-induced activation of core electrons [84]. Their crystal structures display motifs resembling the isoelectronic $[\text{XeF}_n]^-$ molecules – for example, $Fdd2$ CsF_5 contains planar pentagonal CsF_5 units, similar to the $[\text{XeF}_5]^-$ anion. With increasing fluorine content, the formal oxidation state on cesium reaches values greater than +1.

3.2 High Pressure Electrides

Electrides are solids where the electrons, localized on non nuclear-centric sites, behave as anions [85]. They are conceptually related to solvated electrons, in

which the excess electrons can be thought to occupy cavities in the fluid [86], as well as alkalide liquids [41, 42] or alkalide solids where alkali metal anions fill the interstitial voids [74]. Although many types of electride families are known at atmospheric conditions, including those that are organic, inorganic, intermetallic and those where the electron localization is restricted to various dimensions or possesses topological properties, herein, we restrict the discussion to high pressure electrides: systems where the electron localization occurs as a response to compression [87].

Though the formation of high pressure electrides has been rationalized in many ways, including pressure induced orbital rehybridizations [4, 88, 89], and multicenter bond formation [90, 91], herein we focus on a simple model proposed by Miao and Hoffmann [87, 92]. As atoms in a solid compound are compressed, raising their orbital energies, the electrons in the highest-energy orbitals can vacate the atom entirely and occupy the interstices of the crystal lattice instead. To understand why this might occur, Miao and Hoffmann pointed out that orbitals can be ascribed to these voids, which can be thought of as interstitial quasiatoms (ISQs). At ambient pressure, the ISQ energies are higher than the atom-centered ones. However, unlike the atom-centered orbitals, those of the ISQ do not experience the repulsive effect caused by the core electrons, and their increase in energy with pressure will be less than the atom-centered orbitals. When the ISQ orbital energies fall below the atom-centered ones they will be occupied, thereby localizing the valence electrons in the interstitial regions. These electrons, detached from the nuclei, serve as anions and the corresponding compounds are called *electrides*.

For several simple metals, high-pressure phases identified as electrides via calculations have been subsequently studied experimentally. In sodium, Neaton and Ashcroft posited that under pressures high enough to induce overlap of the $2p$ orbitals, a combination of Pauli repulsion and core orthogonality constraints would drive the valence electrons away from the ionic cores, to localize in the crystalline interstices instead. This electronic redistribution would result in a metal-to-insulator transition [88]. Later CSP calculations – with experimental confirmation of an optically transparent, wide-bandgap insulating phase in the same publication – proposed an insulating $hP4$ phase with $P6_3/mmc$ symmetry to become stable above 260 GPa. [4] The new $hP4$ phase was in fact experimentally observed at pressures as low as 200 GPa, but the discrepancy was ascribed to a combination of thermal effects as well as the preferential stabilization of metallic states by the computational method employed. Moving to higher pressures and temperatures, evidence for the $hP4$ phase has been obtained in shock-ramp experiments [5]. However, *in situ* X-ray diffraction (XRD) revealed peaks that could not be attributed to $hP4$ between 240-325 GPa at temperatures in the thousands-of-degrees Kelvin. Consistent with these dynamic compression experiments, calculations showed that the free energy of a $P6_3/m$ symmetry phase that is a topological electride was lower than that of $hP4$ at these pressures and temperatures [93]. At higher

pressures yet, ca. 15.5 TPa, sodium is predicted to adopt a curious, metallic *cI24* electride phase consisting of Na₁₂ icosahedra [94]. In the insulating *hP4* structure that dominates much of the high-pressure landscape in sodium, highlighted in Figure 4a, the atoms occupy the Ni sites of the Ni₂In structure type with the ISQs on the In sites, in line with the treatment of this phase as (Na⁺)₂E²⁻ (where E²⁻ denotes a doubly-occupied ISQ). In fact, several A₂X alkali metal chalcogenides adopt the antiferroite *Fm* $\bar{3}$ *m* crystal structure at ambient conditions, but eventually transition to the Ni₂In structure type under pressure [95, 96]. Potassium also adopts the *hP4* phase when squeezed [62, 97].

Lithium presents another example of complex structural and electronic behavior under pressure, as first postulated by Neaton and Ashcroft who suggested it may adopt an insulating, paired ground state [59]. Subsequent experiments revealed that Li assumes the same semimetallic *cI16* [60] structure found in Na [98]. At higher pressures, Li transitions to a number of unique phases, such as those with orthorhombic C-centered lattices and 88, 40, and 24 atoms in their unit cells which have been observed [99]. One of these, *oC40* with the *Aba2* space group, is an electride displaying especially interesting behavior [100]. In this phase, ISQs occupy three separate symmetry-distinct sites, two that are doubly occupied (E^{II}) and the third singly occupied (E^I), so its primitive cell can be considered as Li₂₀E₈^{II}E₄^I. The E^I-E^I distance remains roughly constant at a short 1.3 Å from 50-80 GPa, with an elevated electron density found between the ISQs. Crystal Orbital Hamilton Population (COHP) [101], ELF, and projected density of states (PDOS) analyses all indicate bonding character between the E^I sites, and examination of the Γ -point band-decomposed charge densities revealed bonding and antibonding states analogous to the σ_g and σ_u^* orbitals in H₂. In fact, computations have shown that ISQs can form covalent, ionic and metallic bonds with atoms as well as with other ISQs [87, 89, 100, 102, 103]. For this reason, Miao has espoused the idea that ISQs may be thought of as a chemical element and placed above helium in the periodic table under pressure [104].

The proclivity of the elements to ISQ formation has been investigated by comparing the energies of their orbitals calculated at different pressures using a He confinement model with those of an ISQ 1s orbital [92]. Unsurprisingly, Li and Na were found to favor ISQ formation at relatively low pressures, with Mg, Al, In, and Tl predicted to follow suit at higher pressures. Among the heavier alkali metals, the energies of the valence s orbitals were found to rapidly increase in energy relative to that of the ISQ 1s – but as previously discussed, these elements are also susceptible to a pressure induced electronic $ns \rightarrow (n-1)d$ transition. Within cesium, for example, the increased d occupation, already noted by Sternheimer in 1950 [53], was invoked to explain the curious structure of Cs-IV adopted at 4.3 GPa, where the Cs atoms possess a coordination number of 8 [55]. This decrease in coordination number with increasing pressure appeared so counterintuitive to Linus Pauling that he presented an alternative structure solution assuming cubic symmetry and invoking icosahedral clusters [105]. Pauling’s hypothesis turned out to be incorrect.

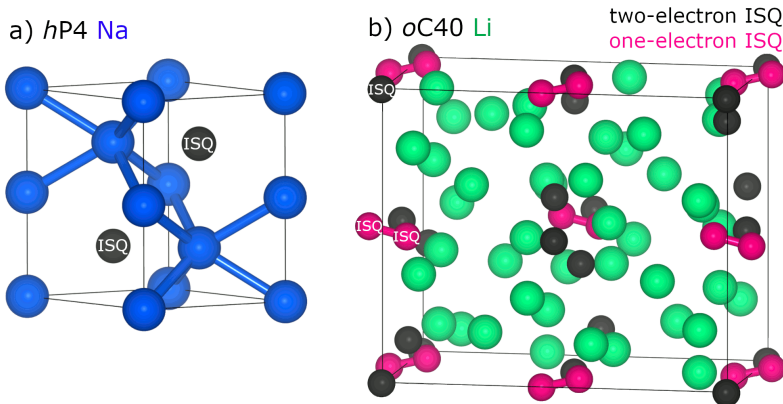


Fig. 4 High pressure electride formation is observed in a number of complex high-pressure phases of the alkali metals, including both the insulating (a) *hP4* phase of Na [4] (Ni_2In structure type) where ISQs containing two electrons occupy the In sites, and (b) semiconducting *oC40* Li, containing three inequivalent ISQ sites of which two (black) are doubly occupied, and the third (pink) is singly occupied so a bond is formed between nearest neighbors, as highlighted by the lines that join them.

Importantly, von Schnering and Nesper [106] recognized that the Cs atoms in the Cs-IV structure occupied the Th sites of the ThSi_2 lattice – and that the valence electron density exhibited maxima not near the Cs atoms but at the Si positions of ThSi_2 and between the Si-Si bonds, dubbing this phase an electride. This $I4_1/amd$ structure is also assumed by K and Rb under pressure [107–109].

If the high-pressure phase behavior of the alkali metals were not complex enough, Na, K, and Rb all adopt different versions of an incommensurately modulated host-guest lattice (similar to the W_5Si_3 type), often referred to as the *tI19* structure, a model of which is illustrated for K in Figure 2d. [4, 65, 107, 110–114] All three share the same host lattice, but display different periodicity in the guest lattice. In a study using commensurate approximants to model the electronic structure, electron localization in the interstitial spaces was found, with some highly localized basins as well as a 1D channel of electron density lying in channels of the host structure [114]. Another study proposed that electrides in the heavy alkali metals could be stabilized via ferromagnetic ordering [75].

Numerous predicted binary and ternary systems under pressure also behave as electrides, including two Li_3Fe phases (with $P6/mmm$ and $P4/mbm$ symmetries) [115], $P4/mbm$ Na_3Fe [116], and a superconducting Y_3Si phase [117]. In a range of Li_nI stoichiometry phases predicted above 50 GPa, ISQs form within the interstices between I-centered Li polyhedra – but higher pressures drive electron density back from the ISQs to the iodine atoms, filling the 5p and eventually the 5d orbitals, skipping the 6s, in line with disfavoring s orbital occupation under pressure [103]. Finally, several electride phases have been

identified involving the famously unreactive noble gases - including a particularly surprising case [10] where the noble gas is crucial to the stability of the synthesized structure.

3.3 Compounds of noble gases

Where did all the xenon go?

Relative to the abundance of Ar and Kr in the Earth's atmosphere, the amount of Xe is strikingly lower than it should be, a problem known as the "missing xenon paradox". Geoscientists have explained this discrepancy in many different ways [118–120], but a growing body of evidence suggests that the Xe did not escape, and instead it has been incorporated into the minerals found within the Earth. At Earth's core pressures, both the atomic orbital energies and the relative electronegativities of the elements, including Xe and the Fe and Ni that comprise the majority of the core, are significantly perturbed [48, 50]. Therefore, it should not be a surprise that their reactivity differs from our 1 atmosphere expectations.

Prior to the advent of widespread CSP, computational investigations concluded that Xe incorporation into Fe and Ni would not occur, at least not to a large extent [121, 122]. These studies, which relied on the assumption that the Xe-metal alloys adopted crystal lattices similar to those of the elemental metals, turned out to be incorrect. Later CSP-based studies predicted the emergence of stable Xe-Fe and Xe-Ni compounds above 250 and 200 GPa, respectively [123], with $Pm\bar{3}m$ XeFe₃ (AuCu₃-type) and $Pm\bar{m}n$ XeNi₃ (based on Xe@Ni₁₂ cubooctahedra) having the lowest enthalpies of formation, although $P\bar{6}2m$ XeFe₅ and XeNi₅, as well as $P2_1/m$ XeNi₆ also appeared on the convex hull. Confirming these predictions, experimental studies have synthesized XeNi₃ and Xe(Fe/Ni)₃ phases at high pressure, although with slightly different structures than those predicted. This includes $Pm\bar{3}m$ for XeNi₃, either as an ordered AuCu₃ [67] or disordered CrNi₃ alloy [68], and a mixture of *fcc* and $Pm\bar{m}n$ -symmetry phases for XeFe₃ [68]. In these systems, the Fe and Ni atoms behave as oxidants, accepting 5p electron density from Xe [68, 123], in agreement with the predicted increase in electronegativity differences between Xe and the transition metals at high pressure [50]. Xe₂FeO₂ and XeFe₃O₆, both involving substantial Fe-O and Xe-O bonding, have also been computed to be stable at pressures relevant to the Earth's core [124]. The high-pressure ArNi phase, in which some Ni 3d electron density is transferred to the Ar 4s, inducing a magnetic moment on the Ni, has been synthesized [125].

CSP calculations have also predicted stable compounds containing Xe, or other noble gas (NG) elements, and Mg above 125-250 GPa [102]. This includes Mg-Xe and Mg-Kr phases, which adopt structures based on stacked square lattices of Mg and the NGs in different patterns, ranging from the CsCl type ($Pm\bar{3}m$) to more complex $P4/nmm$ or $I4/mmm$ arrangements for MgNG and Mg₂NG stoichiometries. Compounds of Mg with Ar, on the other hand, were found to favor hexagonal arrangements such as anti-NiAs type MgAr ($P6_3/mmc$). In these compounds the energies of the metal 3s orbitals

increase precipitously in comparison to the outer shell d orbitals of the noble gases inducing Mg 3s \rightarrow NG d orbital transfer. The ELF of Mg₂NG (NG=Xe, Kr, and Ar) phases shows an additional interesting feature: ISQ formation. This occurs far below the pressures at which elemental Mg is predicted to form an electride [89, 92]. Two reasons have been used to explain this phenomenon [102]. First, far fewer ISQ sites – concomitantly occupying less space – relative to the elemental Mg electride are necessary to accept the displaced valence electrons of Mg, as many of them are transferred to the NG atoms instead. In addition, the NG atoms promote the formation of larger interstitial spaces in the structure, stabilizing the ISQ at lower pressures. Under moderate pressures of ca. 50-300 GPa, the energies of the outer shell Xe d orbitals are similar to those of the ISQ 1s, although with higher pressure they become lower in energy, congruent with the gradual ISQ 1s \rightarrow NG d electron transfer with increasing pressure up to 600 GPa [102].

Several other stable compounds of Xe have been predicted at high pressures, including XeO, XeO₂, and XeO₃ [126], as well as Xe₃O₂, Xe₂O, and Xe₇O₂ [127], while Xe₂O₅ and Xe₃O₂ have both been experimentally observed at pressures lower than 100 GPa. [128] Krypton oxide, KrO, has been predicted as well [129], as have xenon nitrides [130, 131] and carbides [132]. Fluorides of argon [133], krypton [134], and xenon [135] – with Xe-Xe dimers cropping up in Xe₂F and XeF – have all been predicted. Several xenon chlorides including XeCl, XeCl₂, and XeCl₄, with the former two being metastable by 10 GPa and reaching the convex hull by 60 GPa have been computationally studied [136]. When they are combined with Li, the noble gases Ar [137] and Xe [138] are predicted to behave as anions, with the Li 2s orbital rising above the Xe and Kr outer shell d orbitals. Several cesium xenides are predicted to be stable at high pressures, many adopting alternate colorings of a distorted bcc lattice [139]. There is experimental evidence for the formation of a phase mixing Xe with water ice at conditions expected for planets such as Uranus and Neptune [140].

Helium is famously the most inert element at ambient pressure by virtue of its closed-shell electronic configuration, zero electron affinity and large ionization potential. Nonetheless, a number of stable helium-containing compounds have recently been predicted at high pressure, including those with iron [141], ammonia [142], water [143, 144], nitrogen [145, 146], and even with *other noble gases* [147, 148] (the van der Waals compound NeHe₂, a Laves phase in the MgZn₂ structure has been experimentally observed [149]).

A particularly noteworthy example is provided by Na₂He [10], an electride phase with a fluorite-like lattice (Figure 5a) in which every Na₈ cube that does not contain a He atom is instead occupied by an electron pair (Figure 5b), so that the phase can be expressed as (Na⁺)₂(E²⁻)He. Although He does not participate in any bond formation, its presence is nevertheless a crucial stabilizing force in this phase, which has been successfully synthesized above 113 GPa [10]. A subsequent computational study showed that the He atoms act as inert “spacers” to reduce the Madelung repulsion resulting from the unequal amounts of cations and anions in the parent (Na⁺)₂(E²⁻) phase [150]. Reaction

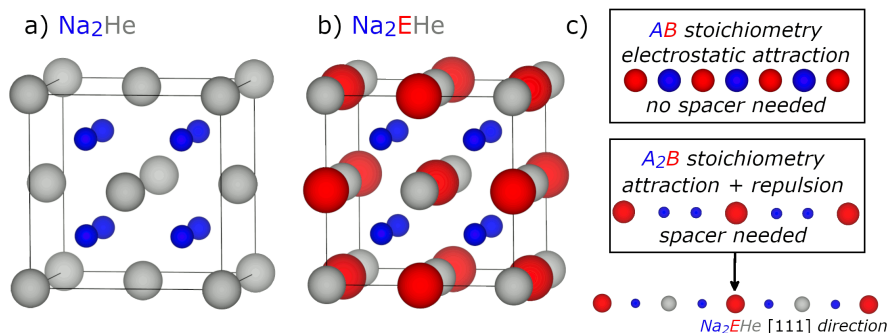


Fig. 5 Conventional unit cell of helium-containing Na_2He [10] in the $Fm\bar{3}m$ space group (a), an electride with localized electron pairs occupying octahedral vacancies (b). The mechanism by which He incorporation serves to stabilize the structure is illustrated in (c), which shows schematically how He insertion reduces electrostatic repulsions involved in the A_2B (Na_2E) stoichiometry.

enthalpies for helium in combination with ionic AB, A_2B and AB_2 compounds revealed that He incorporation was generally favored when the cation:anion ratios were unequal such as in MgF_2 and Li_2O , but not for AB-type phases such as LiF or MgO , in line with the prediction of successful He incorporation into certain alkali oxides and sulfides [151]. Helium placement in the ionic lattices tends to separate ions of similar charge as shown schematically in Figure 5c. An FeO_2He phase in which the Fe and O atoms form a fluorite lattice and the He atoms occupy the remaining Fe_8 cubes (isopointal to Na_2EHe) was predicted to be stable above 120 GPa [152], with He appearing to play the same role of spacing agent. This mechanism allows even the most inert noble gases to play an active role in stabilizing compounds at high pressure, all without forming a single chemical bond.

3.4 Miscibility under pressure

The noble gases obtained their names due to their general lack of reactivity, but under ambient conditions, numerous combinations of elements resist mixing to form alloys or stoichiometric compounds. The proclivity or reluctance of a pair of elements towards mixing has been explained in a variety of ways, resulting in predictive rules including those of Hume-Rothery and co-workers [153], Miedema’s model [154, 155], Darken and Gurry’s maps [156], and more [157–159]. As we will soon see, pressure turns out to be a useful variable that can alter the (im)miscibility of two or more elements.

Consider, for example, magnesium and iron, whose large size and small electronegativity differential at ambient pressure makes compound formation intractable [160]. According to Miedema’s rules, compound formation is favored by large electronegativity differences and similar charge densities [154]. The electronegativity difference between the two elements greatly increases under pressure [48, 57] – and because Mg is more compressible, its radius

approaches that of Fe when squeezed, thereby increasing the miscibility of the two elements. As a result, stable Mg-Fe compounds have been computationally [161, 162] and experimentally [163] studied under pressure. The higher compressibility of K has also been found to favor compound formation with transition metals such as Ag, even at pressures below which K is anticipated to undergo an $ns \rightarrow (n - 1)d$ transition [7].

Another case-in-point of pressure induced reactivity are the Li-Be alloys predicted to be stable in the megabar regime [164]. By 20 GPa LiBe_2 reaches the Li-Be convex hull, where it is joined by LiBe_4 (shown in Figure 6a) and LiBe by 80 GPa. At 100 GPa the latter trades its place on the convex hull with Li_3Be . Alignment of strong diffraction peaks with $2k_F$ (twice the free-electron Fermi wavevector) is suggestive of stabilization through a Fermi surface-Brillouin zone interaction mechanism, which has been used to explain the particular stabilities (and electron counts which make them so) of Hume-Rothery electron phases [165, 166]. Furthermore, at around 82 GPa, an odd feature emerges in the DOS curve of $P2_1/m$ LiBe : the base of the valence band appears as a step-like function, remains flat for ~ 4 eV, and sharply increases once more before more complex features take over. This is linked to a distinct separation – made possible by the pressure-induced increase in the electronegativity difference between Li and Be – between high- and low-electron density planes associated with the Be and Li atoms, respectively, leading to quasi-2D-like behavior in a geometrically 3D structure. Stabilization through Fermi sphere interaction with higher zones (referred to as Jones zones from the Mott-Jones formulation of this mechanism) was invoked to propose a high-pressure NaAl phase in the NaTl structure type [167] just above 12 GPa.

Another element that does not undergo compound formation with Li at ambient conditions is Fe. Just above 40 GPa, however, Li_3Fe ($P6/mmm$) and LiFe ($Fd\bar{3}m$, NaTl -type) phases are computed to lie on the convex hull [115]. Some interstitial electron localization appears in Li_3Fe , both in $P6/mmm$ symmetry as well as the $P4/mbm$ symmetry computed to prevail just above 60 GPa which is shown in Figure 6b. Both Li_3Fe phases are host-guest lattices, with the Fe atoms lying in larger hexagonal ($P6/mmm$) and heptagonal ($P4/mbm$) channels, and the electron localization is found within the smaller triangular and square channels. Na_3Fe is predicted to adopt this same $P4/mbm$ phase between 120 and 300 GPa [116]. An additional Li_3Fe_2 phase with $C2/m$ symmetry appears on the convex hull by 80 GPa, involving Fe zigzag chains in combination with alternating Li linear or armchair chains.

Recently, a host of bismuth-containing phases have been found to be stabilized at high pressure. Bismuth is a component in numerous topologically nontrivial materials [170, 171] and superconducting systems at ambient pressure [172–174], yet under these conditions does not form stable compounds with many of the transition metals. In combination with the exotic bulk properties of bismuth, the various magnetic or otherwise electronically nontrivial properties of the transition metals make for a tantalizing combination in high pressure experiments. Under pressure, the estimated electronegativity of Bi

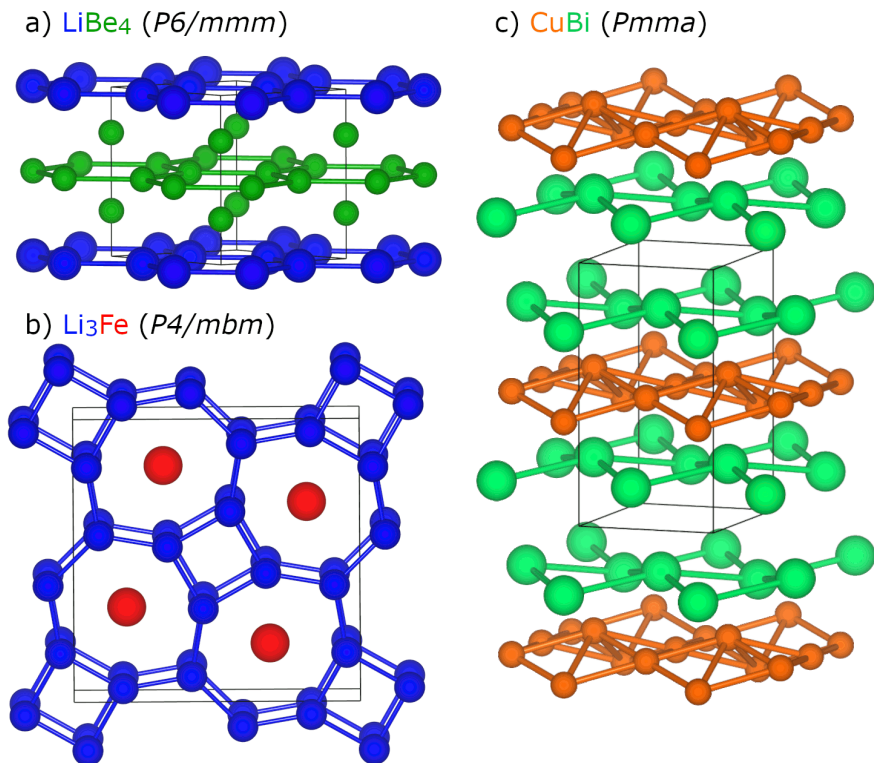


Fig. 6 High pressure enables the mixing of elements which do not form compounds or alloys otherwise. These include (a) LiBe_4 , a layered compound of Li and Be [164], (b) Li_3Fe , a host-guest compound with Fe atoms as the guests to a Li-based host lattice [115], and (c) CuBi [168, 169], one representative of the many bismuth-containing compounds which have been found at high pressure. CuBi has been experimentally observed.

drops precipitously in comparison to most of the d-block, rendering it more reactive [48, 57]. Indeed, above 32 GPa, FeBi_2 [175, 176] was observed to form in DAC experiments in the $I4/mcm$ Al_2Cu structure type shared by NiBi_2 [177] and MnBi_2 [178] (both are stabilized by high pressure although other Ni-Bi and Mn-Bi phases are accessible at atmospheric pressure), as well as certain high-pressure transition metal pnictides [179–181]. A second phase, FeBi_3 with $Cmcm$ symmetry, has also been predicted to lie on the convex hull between 36 and 39 GPa, but this narrow stability range likely hinders synthetic accessibility [176].

In fact, high-pressure high-temperature methods have been used to synthesize a wide variety of bismuth-containing compounds including CoBi_3 [182, 183], which adopts the $Pnma$ NiBi_3 structure type, becomes stable by 5 GPa, and is a superconductor with a T_c just below 0.5 K. Synthesized binaries of Cu and Bi include $\text{Cu}_{11}\text{Bi}_7$ at 3 GPa [184] and CuBi (Figure 6c) at 6 GPa [168, 169], as well as a $I4/mmm$ Cu_2Bi phase above 50 GPa [185], which

is possibly overtaken by a Cu_7Bi_2 phase [177]. Of the second-row transition metals, MoBi_2 , also in the Al_2Cu structure type, has been synthesized above 35 GPa, while evidence for a Mo-Bi bcc-type alloy appeared above 5 GPa [186].

The Linear Approximation to Enthalpy (LAE), a tool for rapid and computationally cheap evaluation of formation enthalpies, was used to explore the high-pressure stability of structures in binary ambient-immiscible systems [177]. In concert with the minima hopping CSP method, several new phases were found to be stabilized by 50 GPa: PbAs , Si_3Al , SiAl , SiAl_3 , BiSn_3 – yet another bismuthide – In_3Fe , Hg_3In , HgIn , HgIn_3 , Hg_3Sn , ReSn_3 , ReBr_3 , ReGa , and ReGa_3 . Only a limited range of stoichiometries (A_3B , AB , and AB_3) was sampled, encouraging further investigation into each of these systems – but now there is preliminary data to suggest fertile ground.

3.5 Geometries and bonding

In the previous sections, we have explored curious electronic interactions made possible by external pressure and compound formation between unexpected species. Here, we shift our focus to the particular geometrical arrangements that emerge in materials under pressure. With higher density, atoms are forced into closer proximity – the possibility of electrone formation notwithstanding – which can promote multicenter bonding in both electron-poor and electron-rich contexts as coordination numbers increase [13]. When electron-precise species are closely bunched under compression, electron-deficient multicenter bonding can emerge as the constituent electrons are needed to span more bonding interactions.

Bond symmetrization is a frequent secondary consequence of compression: an asymmetric fragment forced to occupy a progressively smaller space has less room for asymmetry. Often, this leads to a collapse into a symmetric and multicentered bonding regime, as was predicted for water ice under pressure by Pauling [187]. He suggested that the intermolecular hydrogen bonds between adjacent water molecules would shorten with pressure [187], eventually becoming equivalent with the intramolecular O-H bonds, as illustrated in Figure 7a. This prediction was verified experimentally upon the discovery of ice X, where the lone pairs of the oxygen atoms are used to form additional covalent bonds, rendering the oxygen atoms tetrahedrally coordinated by hydrogens in a diamond-like network [188, 189]. Pressure-induced hydrogen bond symmetrization has also been observed in computations on hydrogen halide systems such as HF, HCl and HBr [190], as well as in the record-breaking superconductor $\text{Im}\bar{3}m$ H_3S [191].

Small homoatomic clusters alien to the 1 atmosphere pressure-trained mind are found or predicted for other elements in high pressure crystal structures. The wide structural variety has been explained by the increased stabilization of homonuclear bonds as compared to more polar or ionic bonds under pressure [104], favoring single-element clustering. An example of a compound containing novel homonuclear motifs is Pnma NaCl_3 (Figure 7b), computed to be stable from 20 to 48 GPa, featuring a linear Cl_3^- anion reminiscent of

the more familiar triiodide I_3^- [9]. Another such motif is the pentazolate N_5^- ring, which can store more energy than the related azide anion N_3^- , but is challenging to synthesize at ambient pressure [192, 193]. This species, ubiquitous in high-pressure phases, is predicted to be a constituent of LiN_5 [194–197] – a phase that has been successfully quenched to ambient conditions after synthesis at 45 GPa [198] – to sodium pentazolates NaN_5 and Na_2N_5 [199], CsN_5 [200], CuN_5 [201], MgN_{10} and BeN_{10} [202], ZnN_{10} [203], BaN_5 and BaN_{10} [204], SnN_{20} [205], and IrN_7 [206]. Polynitrogen chains feature in many proposed high-pressure compounds of Cs [200], Fe [207], Zn [203], Ba [204], Sn [205], Cd [208], Gd [209], and Ta [210], the last of which has been experimentally realized. High pressure also facilitates the formation of silicon clusters in predicted phases including Si_4 squares in $CaSi$ [211], extended networks and clathrate-like cages in silicides such as $CsSi_6$ [212], $MgSi_5$ [213], and several lithium silicide compounds [214].

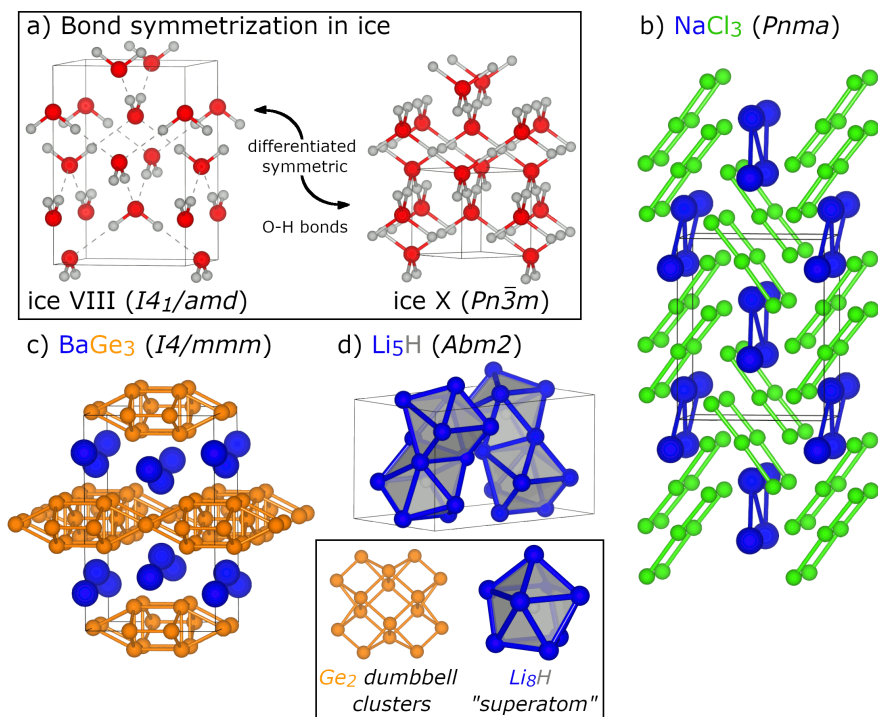


Fig. 7 Geometrical and bonding adaptations at high pressures. With pressure (a), covalent O-H and intermolecular hydrogen bonds between separate water molecules in the ice VIII phase equilibrate to yield the symmetric ice X phase [188, 189]. Pressure coincides with the appearance of strange motifs including (b) linear trichloride anions in $Pnma$ $NaCl_3$ [9], (c) clusters of Ge dumbbells (inset) in $I4/mmm$ $BaGe_3$ [215, 216], and (d) Li_8H “superatom-like” building blocks (inset) in $Abm2$ Li_5H [217]. Except for Li_5H , all have been experimentally realized.

Tetrel clusters comprise a family of polar intermetallic $I4/mmm$ symmetry compounds formed from alkaline earth or rare earth metals and group 14 tetrrels in a 1:3 ratio. An example of these isotypic compounds, BaGe_3 , is shown in Figure 7c. The clusters within it may be described as tetrel dumbbells condensed into cubes, which are capped on four equatorial faces by additional dumbbells shared with a neighboring cube, forming a loose three-dimensional network. This structure has been experimentally observed in Ca, Y, and Lu silicides [218] (and later identified in a CSP investigation of the Y-Si system [117]), and a related distorted $I\bar{4}2m$ BaSi_3 phase has also been synthesized [219]. Alkaline earth trigermanides CaGe_3 [220], SrGe_3 [221], and BaGe_3 [215, 216] have also been found to adopt this structure. The distribution of electrons within the clusters aligns with two-center two-electron bonds along the tetrel dumbbells, with multicenter interactions between the tetrel and rare earth/alkaline earth [215, 218, 222]. Superconductivity has been measured in some of these compounds, albeit at low temperatures [216, 218], augmented by predictions from first principles calculations [104, 117, 222]. Additionally, the stability conferred by the strong covalently bonded networks permits some of these phases, synthesized at high-temperatures and high-pressures, to be recovered at ambient conditions [219, 222]. A similar example is presented by elemental carbon – diamond is its ground state at high-pressures, but due to the immense strength of its sp^3 covalently bonded network, the energetic barrier for its transition to the lower-enthalpy allotrope graphite is too high and it persists “forever” under ambient conditions. Furthermore, laser-driven ramp compression studies of carbon to 2 TPa have found that carbon stubbornly maintains the diamond structure well beyond its predicted high-pressure stability limits [223], as the barriers to breaking the sp^3 bonds remain large under pressure.

Another example of unique clusters predicted to form only at high pressures are found within a family of lithium subhydrides [217]. Computations uncovered two nearly isoenthalpic Li_5H phases that had the most negative enthalpies of formation. Both were built of Li_8H units that behaved as superatoms analogous to similar units in synthesized Rb_9O_2 and Cs_{11}O_3 suboxides [224]. One of these, with $Abm2$ symmetry, is shown in Figure 7d. The Li_8H cluster, a distorted bicapped trigonal antiprism of Li encapsulating a single H atom, has one electron in excess of the closed-shell octet and thus behaves as a superalkali atom.

In addition to the well-known H_2 molecular units and H^- hydridic species, hydrogen atoms can form other distinct clusters. One of these, the trihydrogen cation, H_3^+ , is in fact one of the most abundant species in the universe – but it is also largely relegated to interstellar space and the atmospheres of gas giant planets [225]. High pressure crystal chemistry offers another opportunity. The halogen polyhydride Cc H_5Cl [226–228], predicted to become stable above 100 GPa, contains slightly distorted H_3^+ clusters with H-H distances of 0.74, 0.97 and 1.01 Å [226]. By 300 GPa the three distances converge to 0.87–0.88 Å, yielding a nearly-perfect equilateral triangle. With sufficient pressure, this H_3^+

unit interacts with a neighboring H₂ molecule forming a twisted bowtie-like loosely interacting H₅⁺ motif [226, 228]. Metastable predicted H₂F, H₃F, and H₅F species, as well as H₅Br also contain this triangular H₃⁺ cation [227], as does the metastable *P1* LiF₄H₄ [229].

With two extra electrons, the trihydride anion, H₃⁻, prefers a linear arrangement involving a three-center four-electron bond. Quantum chemical calculations have shown that the ground state geometry of the isolated trihydride anion possesses one H-H bond that is substantially longer than the other (2.84 vs. 0.75 Å), with the transition state between the H-H · · H and H · · H-H configurations corresponding to the symmetric case [230]. Nevertheless, certain predicted high-pressure hydrides of the heavy alkali metals K [66], Rb [231], and Cs [232] (as well as the alkaline earth metal Ba [233]) feature an H₃⁻ anion symmetrized via pressure. Synthesized NaH₇ is thought to contain an asymmetric linear H₃⁻ motif [234]. Linear H₃⁻ units are also predicted to appear in various indium [235] and lithium polyhydrides [236].

Scandium polyhydrides, meanwhile, are predicted to feature five-membered rings of hydrogen atoms in various arrangements. In *I4₁/md* ScH₉, which lies on the convex hull around 300 GPa [237], strips of edge-sharing H₅ pentagons are stacked perpendicular to one another along the *c* axis, linked by vertices. The strips are separated by additional H atoms in molecular H₂ units. Around 250 GPa, ScH₁₀ adopts a *Cmcm* structure in which H₅ pentagons are grouped into sets of three, sharing edges and a single common vertex. This phase is nearly isoenthalpic with another ScH₁₀ structure with the same (H₅)₃ “pentagraphenelike” clusters but arranged in *P6₃/mmc* symmetry [238]. ELF demonstrates bonding within the H₅ units [237, 238]. This same pentagraphenelike structure is expected to lie on the Lu-H convex hull at 300 GPa and to be very near the Hf-H and Zr-H hulls [238]. For higher hydrogen contents yet, ScH₁₂ is predicted to be built of stacked strips of edge-sharing H₅ pentagons spaced by Sc [237].

Indeed, the first, most simple, element does not like to be outdone! One more class of high-pressure hydrogen rich materials whose prediction sparked tremendous experimental synthetic efforts are the so-called “metal superhydrides”. The reason why scientists have pursued them in earnest is the prediction, verified by recent experiments, of conventional superconductivity at temperatures approaching those experienced in a cold room (the *T_c* of LaH₁₀ is about 10 °F – January in Siberia), or a crisp fall day (the *T_c* of C-S-H is about 60 °F), albeit still at very high pressures! CSP investigations into the high-pressure Ca-H system revealed a curious *Im $\bar{3}m$* CaH₆ phase (Figure 8a) stable above 150 GPa in which the Ca atoms were arranged in a bcc lattice and the H atoms condensed into a sodalite-like H₂₄ framework [73]. All H-H distances were equivalent, 1.24 Å at 150 GPa, and ELF analysis confirmed weak covalent bonding between the H atoms. This phase, a good metal, was predicted to exhibit large electron-phonon coupling, and indeed first principles

calculations estimated a superconducting transition temperature T_c of 220–235 K at 150 GPa. Subsequent synthetic exploration led to measurement of T_c over 200 K at 160–170 GPa for CaH_6 [71, 72].

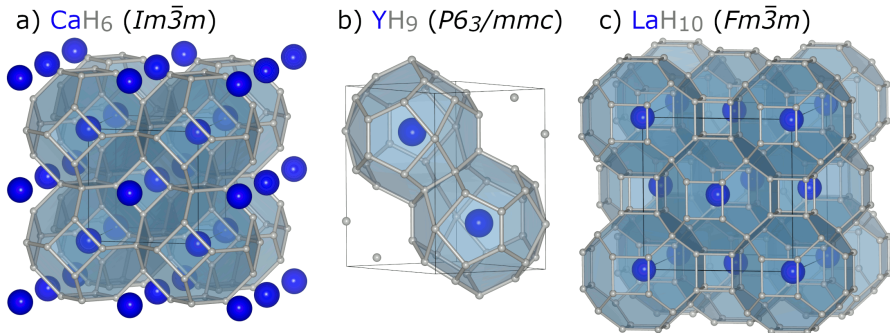


Fig. 8 Clathrate-like metal hydrides predicted then synthesized at high pressures. Their remarkable superconducting properties are tied to strong electron-phonon coupling. Several metal-hydrogen stoichiometries adopt these so-called “superhydride” motifs, including $Im\bar{3}m$ MH_6 , exemplified by CaH_6 [71–73], (b) $P6_3/mmc$ MH_9 , exemplified by YH_9 [35, 69], and (c) $Fm\bar{3}m$ MH_{10} , exemplified by LaH_{10} [34, 35, 37, 70].

The computational discovery of CaH_6 was shortly followed up by fruitful theoretical investigations into related metal-hydrogen systems, turning up isostructural phases for Mg [239], Sc [237, 240, 241], Y [34, 35, 242], Pu [243], Tb [244], Eu [245], and Pm–Lu [246]. Structures that are distortions of this high symmetry phase have been predicted as well. This includes a tetragonally-distorted $I4/mmm$ ZrH_6 variant [247], along with an $R\bar{3}m$ phase in which opposite hexagonal faces of the H_{24} cubic sodalite framework are opened for SrH_6 [248–250] and LaH_6 [34, 35], although the latter may not lie on the convex hull. $Imm2$ BaH_6 [233], which contains some of the H_3^- trihydride anions explored above, can be thought of as a highly fragmented version of the sodalite framework. The role of distortions of the high-symmetry $Im\bar{3}m$ structure adopted by CaH_6 tends to reduce the density of states at the Fermi level, E_F , thereby also lowering T_c . The origin of such distortions has recently been investigated using the lens of DFT-Chemical Pressure [251].

Higher hydrogen content allows for other clathrate-like arrangements of hydrogen, from $P6_3/mmc$ YH_9 [35] (Figure 8b) to $Fm\bar{3}m$ LaH_{10} [34, 35] (Figure 8c). Distorted versions of these two structures have also been predicted, including $C2/m$ CaH_9 [252] and $P1$ Eu_4H_{36} [245], as well as $R\bar{3}m$ CaH_{10} [252] and AcH_{10} [253]. In the case of LaH_{10} , quantum anharmonic effects were found to be key in stabilizing the $Fm\bar{3}m$ structure over less symmetric variants [254]. Other more complex clathrate-like hydrogenic frameworks have been predicted as well. One example is a diamond-like lattice of Mg@H_{28} clusters intercalated with Li@H_{18} units, which comprise the $Fd\bar{3}m$ $\text{Li}_2\text{MgH}_{16}$ phase. This compound is an example of a “hot” superconductor whose estimated T_c , 351 K at 300 GPa, is well above room temperature [255]. Such materials are

under intense speculation and investigation for their promise towards achieving room-temperature superconductivity, as described in Section 4.3 below.

4 Superconductivity

The 1911 discovery of a phenomenon in which a substance's resistivity can plummet to zero [256] sparked countless investigations and resulted in a Nobel prize for Heike Kamerlingh Onnes, as well as a number of future Nobel prizes (directly or indirectly). The mechanism of superconductivity, and the search for new superconducting materials, has fascinated scientists for over a century. A key parameter for superconductors is the critical temperature, T_c , below which a material becomes superconducting. For a number of illustrative superconducting materials, T_c is plotted against the pressure at which they are stable in Figure 9. Of course, practical applications of superconductivity are limited if temperatures very near 0 K are required, and for some decades the highest known T_c values lingered in the low twenties [257, 258]. This sparked debate regarding a possible natural “cap” on superconductivity around these temperatures [259]. However, a family of cuprates whose superconducting mechanism has yet to be explained were the first to break the liquid nitrogen barrier [260], achieving T_c s over 160 K in the case of pressurized $\text{HgBa}_2\text{Ca}_{m-1}\text{Cu}_m\text{O}_{2m+2+\delta}$ [261].

The 2001 discovery of superconductivity up to 39 K in MgB_2 [263] provided experimental evidence that non-cuprate phases could be promising superconductors, despite the fact that they deviated from the collection of empirical rules enumerated by B. T. Matthias in the 1950s and 1960s [272]. These ranged from favorable valence electron concentrations to a general distrust for theorists. MgB_2 belongs, with early and long-term record holders Nb_3Sn and Nb_3Ge , as well as the clathrate-like hydrides discussed in Section 3.5, to the family of “conventional” superconductors whose mechanism is thought to follow the theory propounded by Bardeen, Cooper, and Schrieffer in 1957 [273, 274]. This discovery revitalized interest in conventional superconductors [275], leading researchers to wonder what the trajectory of superconductivity research would have looked like had the 1957 measurements of the heat capacity of MgB_2 [276] captured the discontinuity that appears upon the superconducting transition.

Within BCS theory, two electrons of opposite momentum and spin that are within $\pm\hbar\omega_{\text{cut}}$ (an energy in line with the phonon energies) of the Fermi surface may, at long distances, overcome Coulombic repulsion and experience a net attractive potential when the lattice is polarized through phonon vibrations. This forms a Cooper pair, a composite boson of weakly interacting species. Thermal energy can break the Cooper pairs, with T_c describing the temperature at which this occurs and the superconducting state is destroyed. From

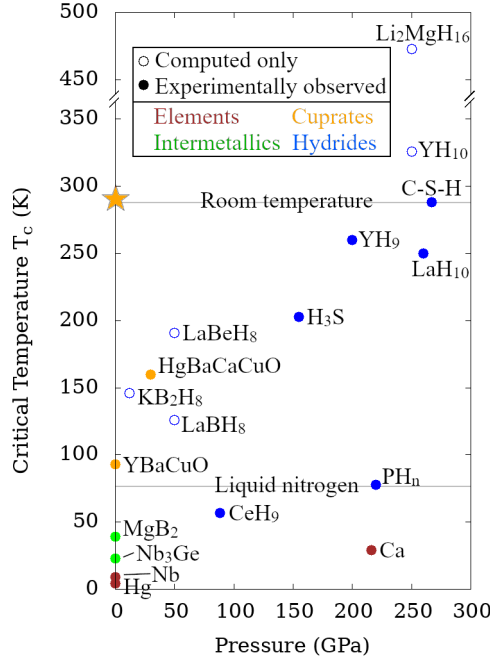


Fig. 9 Critical superconducting temperature, T_c , plotted against pressure for selected materials. Data points based on experimental measurements of T_c are plotted with filled circles, while those estimated via theoretical calculations are plotted with empty circles. Elemental T_c s are given in brown, intermetallics in green, cuprates (belonging to the non-BCS unconventional family) in orange, and hydrides in blue. The boiling point of liquid nitrogen and room temperature are provided to guide the eye, with a star marking the “holy grail” of room-temperature superconductivity at ambient pressure. Data was collected from references [34, 35, 37, 70, 255, 256, 258, 260–271].

this construction, the T_c for a material can be estimated by

$$k_B T_c = 1.14 \hbar \omega \exp \left[\frac{-1}{N_F V} \right] \quad (1)$$

where ω is the average phonon energy, N_F is the single spin electronic density of states at E_F , and V is the pairing potential between two electrons resulting from the electron-phonon interaction. This suggests that high T_c is correlated with a large N_F (a feature potentially tunable via judicious doping), strong coupling between electrons and phonons, and high phonon frequencies. A frequently used semiempirical formula to estimate the T_c of a conventional superconductor is the Allen-Dynes modified McMillan equation [277–279]:

$$T_c = \frac{\omega_{\text{ln}}}{1.2} \exp \left[- \frac{1.04(1 + \lambda)}{\lambda - \mu^*(1 + 0.62\lambda)} \right]. \quad (2)$$

where λ is the electron-phonon coupling constant, ω_{ln} is the logarithmic average phonon frequency and μ^* is the Coulomb repulsion parameter, which is typically treated semiempirically. An approximate – and illustrative – formula to estimate λ was proposed by Hopfield as [280]

$$\lambda = \frac{N_F \langle I^2 \rangle}{M \langle \omega^2 \rangle} \quad (3)$$

where $\langle I^2 \rangle$ are the electron-phonon matrix elements averaged over the Fermi surface, M is the atomic mass, and $\langle \omega^2 \rangle$ the mean phonon frequency. To increase λ , then, N_F and the electron-phonon matrix elements should be increased. Converse to expectations from Equation 1 and Equation 2, where the average phonon energy was directly proportional to T_c , here an increase in $\langle \omega^2 \rangle$ serves to decrease λ . In the denominator of Equation 3, $\langle \omega^2 \rangle$ and M will naturally tend to counteract one another, as increases in atomic mass lead to softer phonon frequencies. In fact, evidence suggests that T_c frequently increases at the edge of dynamic instability, where soft phonons promote strong coupling [281].

In the following sections, we describe the effect of pressure on the propensity for superconductivity of the elements, hydrogen in particular. We end by discussing families of hydrogen-rich phases that are extremely promising towards achieving the once-distant goal of room-temperature superconductivity (albeit potentially only at very high pressures).

4.1 The elements

Most of the elements in the periodic table can be superconducting given the right conditions. This includes, so far without exception, rather low temperatures. However, external pressure can affect the T_c , or even induce superconductivity in some elements [282–285]. In fact, calcium at ambient pressure is not a superconductor and achieves $T_c = 29$ K at 216 GPa [264]. In comparison, the highest elemental T_c at ambient pressure is 9.2 K for niobium [262], while only lithium among the alkali metals [286], and only beryllium [287] among the alkaline earth metals are known to superconduct at ambient pressure, both well under 0.1 K. Of the fifty-four known superconducting elements of the periodic table, only thirty-one are superconductors at ambient pressure.

Early indications regarding the ability of pressure to either enhance or suppress superconductivity [288–290] were less than encouraging. For simple metals whose electronic structure aligns with a mostly free-electron model, such as Zn, Cd, Hg, and the group 13 metals, applied pressure serves to suppress what superconductivity is present at ambient pressure [289, 290]. In such free-electron-like metals, the effect of pressure is to broaden electronic bands and increase phonon frequencies due to the stiffer lattice. Band broadening reduces the electronic density of states at E_F , while a stiffer lattice is correlated

with weaker coupling between electrons and phonons, both effects being detrimental to the superconductivity of a system. At ambient pressure, the alkali metals behave as free-electron metals, but as we have seen in Section 3.2, with pressure their electronic structure rapidly diverges from these expectations.

For Li, T_c is highly pressure-dependent and reliant on complex crystal chemistry [291–293]. Like all of the alkali metals, it adopts a bcc crystal structure at ambient pressure, which in short order transitions to the fcc structure. Up to 8 GPa, the increase in pressure is reflected in an increase in phonon frequencies, typical for a stiffening lattice, but with further pressure the phonons become softer and just above 30–40 GPa, imaginary modes related to a structural instability appear. This pressure corresponds to another phase transition, this time to the $hR1$ ($R\bar{3}m$) structure, and shortly thereafter to the $cI16$. Maxima in T_c are associated with the onset of dynamical instability, as the very soft phonon motions strongly bolster the electron-phonon coupling [281, 294]. From its mostly spherical character at 0 GPa, where lithium adopts a bcc crystal structure, the pressure-induced $2s \rightarrow 2p$ electronic transition drives an increasingly anisotropic Fermi surface featuring *hot spots* of especially strong coupling [295], losing free-electron-like behavior and leading to Fermi surface nesting (FSN) [296–298]. Phonon softening, in particular along the $\Gamma \rightarrow K$ path, is accompanied by enhancement of the electron-phonon coupling [299, 300], with the result that T_c grows from practically zero to a maximum of ~ 20 K. This value is among the higher elemental T_c s, as a result of the pressure-induced electronic transitions in lithium. Following the structural transition to the $cI16$ phase, lithium remains superconducting but T_c decreases due to a reduction of the FSN and concomitant smaller electron-phonon coupling [299, 301, 302]. At high enough pressures, lithium undergoes a metal-semiconductor transition – and eventually goes back to being a (poor) metal upon transitioning to the $oC24$ ($Cmca$) phase [303], but one nonetheless predicted to be superconducting with an estimated T_c of 14 K at 200 GPa [304].

In cesium [305, 306] and rubidium [110, 307], the onset of superconductivity with pressure is associated with the $oC16$ (Cs-V and Rb-IV) structures, alongside the $ns \rightarrow (n-1)d$ transition [307]. An increase in d -character in the electronic states at E_F is correlated with higher T_c in the transition metals [308, 309] and applies here as well to the heavier alkali metals – which, as we have seen, behave under pressure as transition metals themselves.

4.2 Hydrogen

Vitaly Ginzburg, awarded the Nobel Prize in Physics in 2003 for his work in superconductivity and superfluidity, formulated a list of, in his view, the thirty most pressing problems for physics in the 21st century [310, 311]. Following controlled nuclear fusion, the second and third items on this list were high-temperature (room-temperature) superconductivity and metallic hydrogen. These problems are not unrelated.

In 1926, J. D. Bernal proposed that under sufficient pressure hydrogen would transition to a metallic state, but it took nearly a decade for pen to

be put to paper by Wigner and Huntington [312]. Their 1935 suggestion that hydrogen could be metallized by 25 GPa, estimated using a series of assumptions regarding crystal structure and compressibility, proved to be an immense underestimate. In 1968 Neil Ashcroft explicitly linked the quest for metallic hydrogen with the quest for superconductors with higher T_c s, with the suggestion that metallic hydrogen itself would be quite a fantastic superconductor [313]. Hydrogen, being the lightest element, can possess the highest frequencies (as a diatomic molecule) and experience a large electron-phonon coupling due to the lack of screening by core electrons. Moreover, in the metallic state its DOS at E_F is thought to be quite high, making for a very attractive material.

The pressure required to metallize hydrogen, however, is in the multi-megabar range. Claims of metallic or semimetallic hydrogen have been made for DAC experiments at very high pressures and low temperatures, toeing the line of the practical limits of these techniques [314–316]. Complicating the picture, different experiments used different measures to characterize hydrogen’s transition to metallicity, from vibrational spectroscopic techniques such as IR [316], optical measurements such as reflectance and opacity [314], and resistivity measurements [315], as well as different scales to calibrate pressure. At times, this led to seemingly contradictory results, prompting questions regarding experimental accuracy and reproducibility [317–319]. *Ab initio* calculations taking into account the quantum fluctuations of the hydrogen nuclei, however, can reconcile some of these differences, finding in the $C2/c$ -24 high-pressure phase closing of the electronic gap (and transition to metallicity) before the closing of the optical gap (and transition from transparency to reflectivity) [320].

Additionally, the impractically low T_c s of ambient pressure materials are then traded for a much higher T_c in pure metallic hydrogen, but at impractically high pressures! In fact, *ab initio* modeling suggests progressive jumps in T_c with a transition from the molecular (estimated $T_c = 356$ K near 500 GPa) to the atomic phase (T_c increasing to 481 K ca. 700 GPa), and with an atomic-atomic phase transition at ~ 1 -1.5 TPa driving up λ and resulting in an immense estimated $T_c = 764$ K [321]. To address the hydrogen metallization problem, Ashcroft proposed another strategy – instead of pure hydrogen, hydrogen-rich metallic alloys could be targeted as putative superconductors [322]. The presence of additional atoms in the hydrogen matrix would confer a *chemical precompression*, thereby lowering the external pressure required to reach the metallic state. Under ambient conditions, the crystal structures adopted by metal hydrides are largely subject to the dictates of balanced oxidation states, hence alkali metal hydrides assume the rock salt structure, and hydrides of +2 metals favor fluorite or Co_2Si structures, while trivalent metal hydrides tend towards the BiF_3 structure, and so on [323, 324]. Much higher hydrogen content would be needed for such hydrogen-rich alloys, as suggested by Ashcroft, and furthermore many of the resulting structures might differ greatly from anything observed at ambient conditions. Defying the

recommendations of Matthias, the simultaneous and serendipitous advances in CSP methods meant that theoreticians were well poised to answer this call!

4.3 Clathrate-like hydrides

They were successful. As described above, calculations on the high-pressure Ca-H system located the CaH₆ phase described in Section 3.5 [73], in which Ca atoms are embedded into a hydrogenic sodalite-like clathrate framework. The strong electron-phonon coupling predicted for $Im\bar{3}m$ CaH₆ can be traced to breathing and rocking modes of the square H₄ units of the sodalite framework [73]. The molecular orbital diagram for such an H₄ square has, above a filled bonding state, a half-occupied degenerate non-bonding state. Assuming full ionization (integrated charges within atomic basins according to the Quantum Theory of Atoms in Molecules indicate roughly 1 electron per Ca is transferred to the hydrogen network), these orbitals accept the roughly 1/3 electron per H transferred from the Ca atom. This favors symmetry-breaking Jahn-Teller distortions – key contributions to the electron-phonon coupling – that lift the degeneracy.

Similar clathrate-like hydrides, as outlined in Section 3.5, were rapidly predicted in several other systems. $Im\bar{3}m$ YH₆ has been synthesized with a measured T_c of 224 K at 160 GPa [325]. Hydrides with even higher hydrogen content have been synthesized as well, including a $P6_3/mmc$ YH₉ phase with a T_c of 262 K at ca. 180 GPa [69] (a subsequent study reported a slightly lower T_c of 243 K at 200 GPa [326]), and an isotypic CeH₉ phase whose T_c has only been predicted (57 K at 88 GPa and up to 100 K at 130 GPa [35], or 105–117 K by 200 K [267]). The relatively low pressure required to stabilize CeH₉ has been ascribed to strong chemical precompression from the delocalized Ce 4*f* electrons [327]. The reported T_c s for $Fm\bar{3}m$ LaH₁₀ (250 and 260 K at 170 and 185 GPa, respectively [37, 70]), are in line with theoretical predictions of 257–274 K at 250 GPa [34]. Isotypic $Fm\bar{3}m$ YH₁₀ is computed to be a room temperature superconductor with a T_c of 305–327 K at 250 GPa [34]. However, YH₁₀ has thus far eluded synthetic efforts. Partial doping with lanthanum appears to be one strategy to stabilize YH₁₀: a series of ternary (La/Y)H₁₀ phases have been experimentally observed, with measured $T_c = 253$ K [38].

Although the T_c s of many clathrate-like hydrides are stunning, these phases will surely decompose well above atmospheric pressures! CeH₉ is remarkable for the comparatively low, sub-megabar, pressures at which it maintains dynamic stability [267]. In an attempt to preserve the loosely-bound hydrogenic clathrate frameworks that are associated with such strong electron-phonon coupling to lower pressures, one promising strategy involves the addition of a third element in an attempt to further chemically precompress the hydrogenic lattices. The $Fm\bar{3}m$ LaBH₈ phase, which is predicted to maintain dynamic stability down to 40 GPa [269], can be derived from LaH₁₀ by removing two hydrogen atoms per formula unit and placing boron atoms into the center of H₈ cubes that are empty in LaH₁₀ [271, 328]. LaBH₈ has an estimated T_c of 126 K at 50 GPa [269] – and the isostructural LaBeH₈ phase

is predicted to achieve a T_c of 183 K at 20 GPa [271]. Other XYH_8 phases have been proposed, with a variety of possible elemental combinations ripe for tuning stability and properties [271]. A second possibility is afforded by the XY_2H_8 phases that can be constructed by leaving the H_8 cubes empty, but stuffing the center of H_4 tetrahedra instead. KB_2H_8 (dynamically stable to 12 GPa [270]) and LaC_2H_8 (dynamically stable down to 70 GPa [329]) are two representatives of this structural arrangement, with estimated T_c s of 134-146 and 69 K, respectively.

Key to the success of the clathrate-like hydrides is the maintenance of loosely-coordinated networks of hydrogen, rather than condensation into H_2 molecules. The effect of H-H interatomic distances on superconductivity can be seen in the MH_4 hydrides, which adopt the $I4/mmm$ structure shared with ThCr_2Si_2 [330, 331]. Hydrogen occupies two inequivalent sites in the ThCr_2Si_2 structure – the apical H_a (Wyckoff position $4e$, Si) and basal H_b ($4d$, Cr). A plethora of metal hydrides have been predicted or synthesized in this structure type under pressure, including Ca [73, 252, 332] and Sr [248, 249], Sc [237, 240, 241], Y [34, 242], and Zr [247] and rare earths La [34], Ce [35, 267, 333], Pr [35, 334, 335], Pu [243], Tb [244], Eu [245], Nd [35, 336], and Th [337, 338], making systematic study enticing and useful [331]. With metal oxidation states ranging from +2 to +4, the formulas of these compounds can be written as $\text{M}^{x+}(\text{H}_b^-)_2(\text{H}_a)^{-(x-2)-}$, with hydridic H_b and a range of charges possible on the H_a atoms. The T_c s of these phases are correlated with the length of the H_a - H_a contacts, which can behave anywhere from covalently bound H_2 units to fully dissociated hydridic anions depending on the metal atom – similar to the behavior of the X-X bond in ThCr_2Si_2 -type AB_2X_2 phases [339]. The size of the metal atom can be relevant, as larger atoms will stretch the H_a - H_a contact through purely steric interactions, but more important is the valency of the metal atom. Electron transfer from the electropositive metal into the H_a - H_a motif directly populates the H_2 σ_u^* antibonding orbitals, but is also driven by a Kubas-like two-pronged mechanism of H_2 $\sigma_g \rightarrow \text{M } d$ donation, and $\text{M } d \rightarrow \text{H}_2$ σ_u^* back-donation. With enough H_2 σ_u^* population, the H_a atoms behave in a hydridic fashion lowering the T_c , as seen in ZrH_4 [247] and ThH_4 [337]. Donation of sufficient electron density to weaken, but not fully break, the H_a - H_a bonding interaction results in a much higher DOS at E_F and enhanced T_c , as in YH_4 [242].

4.4 Covalent hydrides

The first hydride to top the charts, as it were, was not of the metal clathrate-like family, but instead came from attempts to metallize H_2S . Theory identified an H_2S compound that was computed to possess a T_c of 80 K at 160 GPa [340]. Experimental confirmation followed shortly thereafter, finding a phase with $T_c < 100$ K, but in the process a higher-temperature preparation method yielded a sample with a T_c of 203 K at 150 GPa [266]. A few years before, synthetic exploration into the $(\text{H}_2\text{S})_2\text{H}_2$ stoichiometry found a phase stabilized by pressure-induced hydrogen bonding above 3.5 GPa [341]. This inspired

CSP investigations of the H₃S stoichiometry, which found an $R\bar{3}m$ phase with $T_c = 155\text{--}166$ K at 130 GPa [342]. By 180 GPa this structure transitioned to one with $Im\bar{3}m$ symmetry (Figure 10a) for which the estimated T_c was 191–204 K at 200 GPa. Serendipitously the experimental [266] and theoretical [342] manuscripts appeared at nearly the same time. Subsequent XRD studies supported the identification of the 203 K superconductor as $Im\bar{3}m$ H₃S [343], though other structures have been proposed [344–349].

A host of studies on the H₃S superconductor have followed, exploring the isotope effect, role of anharmonicity, and possible quantum effects [191, 350–359]. The inclusion of quantum nuclear motions lowered the pressure where the less symmetric $R\bar{3}m$ phase was predicted to transition to the $Im\bar{3}m$ structure with symmetric H–S bonds into the range of pressures where high T_c s had been measured [191]. One of the most striking features of the electronic structure of H₃S are a pair of van Hove singularities bracketing E_F [360, 361]. Shifting the position of E_F , potentially by doping, could increase the number of states that can participate in the electron–phonon coupling mechanism, and therefore increase the T_c of the system.

Doping is a common strategy used for precise tuning of E_F , and computations using the virtual crystal approximation (VCA) suggested that the addition of a little bit of phosphorus, carbon, or silicon could raise the T_c into the room-temperature regime > 280 K [362–364]. In the VCA, alchemical pseudoatoms are constructed from weighted averages of the component atom potentials. The resulting chemical chimeras, however, cannot accurately model the local structural and electronic effects that arise when one atom is replaced with an entirely different element. This throws off, in particular, the very dynamical response properties that one must calculate carefully to obtain reasonable estimates of T_c . Additional studies based on actual doped H₃S models constructed as supercells have sought to explore the local effects of doping [365–368], although the calculation of dynamical properties of the requisite large unit cells can be prohibitively expensive.

One particularly promising system involved the addition of carbon to the H₃S lattice by way of methane intercalation [369, 372, 373]. Stoichiometries that are a linear combination of CH₄ and H₃S (the most simple of which is CSH₇) proved especially interesting. They yielded a variety of dynamically stable (although energetically metastable) structures, which differed in the orientation of the methane molecules encapsulated in the H₃S lattice. Some of the highest T_c s predicted for these phases were 181 K at 100 GPa for $I\bar{4}3m$ [372], and 181–194 K for the $R\bar{3}m$ symmetry structure [369] shown in Figure 10b.

Independently, photochemical synthesis in the C–S–H system yielded the first report of room-temperature superconductivity, achieving a T_c of 288 K at 267 GPa [268]. This report has inspired a slew of follow-up work and much debate [371, 374, 375]. XRD analysis performed at pressures below the purported room-temperature superconducting transition [370, 376] is consistent with the Al₂Cu geometry (as well as an orthorhombic $Pnma$ variant) associated with CH₄–H₂ [377] and H₂S–H₂ [341] (Figure 10c). This may suggest an

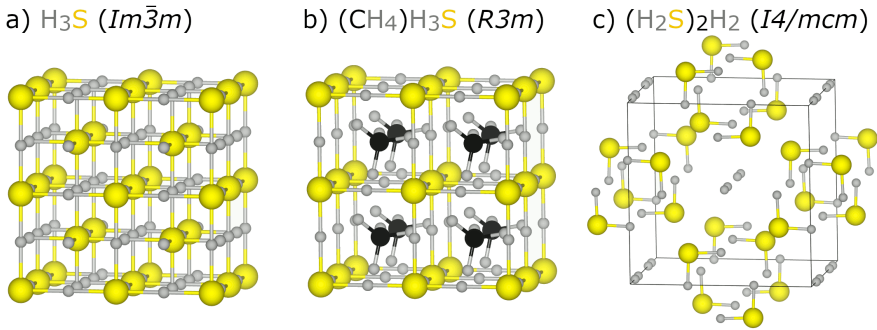


Fig. 10 The covalent hydride $Im\bar{3}m$ H_3S [266] (a) represents a breakthrough in high- T_c conventional superconductivity. Peaks in the electronic DOS near E_F have prompted numerous investigations on doped versions of H_3S , discovering phases such as the methane-intercalated $(\text{CH}_4)\text{H}_3\text{S} = \text{CSH}_7$ [369] (b), among many others. A recent synthesis of a room-temperature superconductor consisting of carbon, sulfur, and hydrogen generated even more momentum, with diffraction analysis performed at pressures below those where the room-temperature superconducting transition were observed, revealing the presence of a phase based on the $I4/mcm$ Al_2Cu -like structure adopted by the van der Waals $(\text{H}_2\text{S})\text{H}_2$ phase [341, 370, 371] (c).

overall stoichiometry of $[(\text{CH}_4)_2\text{H}_2]_x[(\text{H}_2\text{S})_2\text{H}_2]_y$ for the room-temperature C-S-H superconductor, although subsequent phase transitions at higher pressure to the high- T_c superconducting phase cannot be ruled out. In fact, additional studies indicate just such a structural transition occurs to form the room-temperature superconducting phase, with indications of methane signatures in the Raman spectra [371]. As was the case for the binary H_3S system, it appears that a panoply of metastable phases may be accessible by slight variations on synthetic procedure, in particular on carbon content [378], offering plenty of space for further experimental and theoretical discoveries.

In addition to sulfur-based covalent hydrides, phosphorus hydrides have sparked interest after compression of a phosphine (PH_3) sample yielded a material that became superconducting at 30 K at 83 GPa, increasing to 103 K at 207 GPa [265]. The structure and composition of the responsible phase or phases was unclear, prompting an array of follow-up studies levying CSP techniques to identify plausible compounds [379–383]. Pressure was found to drive the decomposition of phosphine into a variety of products with stoichiometries including PH, PH_2 , PH_3 , and more. A predicted $C2/m$ PH_3 phase [380] featuring P-P bonds (in contrast to the H_3S superconductor, which has no S-S bonding) was estimated to be superconducting below 83 K at 200 GPa, in line with the experimental values. Another study suggested that multiple metastable decomposition products of phosphine, including those with PH and PH_2 stoichiometries, might in combination be responsible for the observed superconductivity [382]. PH_2 phases with $C2/m$ and $I4/mmm$ symmetries, differing by a tilt in the component H-P-H moieties, had estimated T_c s of 76 and 70 K, respectively [381]. Later, another set of PH_2 phases were proposed consisting of simple cubic layers of phosphorus capped with hydrogen

atoms and further intercalated with H₂ molecules acting as Coulombic spacing agents [383]. At 80 GPa, these structures had estimated T_c s ca. 30 K, similar to the values that were measured. Raman spectroscopic measurements provided evidence for phosphine dimerization coupled with dehydrogenation under pressure, yielding compositions such as P₂H₄ and P₃H₆ [384, 385]. In these phases, low temperatures were required to maintain stability at multi-megabar pressures. The T_c of a predicted $C2/m$ P₄H₆ phase was estimated to be 67 K at 200 GPa [385].

The plethora of metastable P-H compounds under pressure has prompted computational investigations into ternary systems containing phosphorus and hydrogen. Above 250 GPa, an $R\bar{3}$ LiP₂H₁₄ phase, consisting of P@H₉ clusters spaced by Li atoms as well as isolated H atoms, achieves an estimated T_c of 169 K at 230 GPa (where it is metastable) [386]. $Pm\bar{3}$ LiPH₆, a colored variant of the A15 crystal structure adopted by intermetallic superconductors Nb₃Ge [258] and Nb₃Sn [257], has an estimated T_c of 150-167 K at 200 GPa (where it is metastable) [387]. In the S-P-H system, obviously tantalizing for its connection to the H₃S superconductor as well as to phosphine derivatives, relatively low T_c s were predicted for phases on the high-pressure convex hulls, but low-lying metastable structures based on phosphorus substitution into the $Im\bar{3}m$ H₃S lattice were promising, including $Im\bar{3}m$ S₇PH₂₄, which had an estimated T_c of 183 K at 200 GPa [388].

5 Conclusion

Although the entirety of the lived human experience resides within a vastly narrow pressure range, the universe is not so simple. The chemistry we know at 1 atmosphere is not the chemistry of Jupiter, Saturn, or even the center of our own planet Earth. Starting from the periodic table itself, the ramifications of pressure are rapidly found to alter elemental behavior and, consequently, how the elements interact with one another to form new and bizarre phases. Potassium, in its guise as a “transition metal”, enjoys all manner of new chemical interactions – in compound formation and in the wildly complex electronegative elemental structures it adopts. Cesium can become anionic, and helium takes an active role in stabilizing a network of sodium and interstitial quasiatoms. Strange geometrical and bonding motifs from clusters to networks abound.

Yet not only are the structures of phases – electronic and crystalline – molded by high pressure, but high-pressure studies have revolutionized the search for high-temperature superconductivity. Pressure induces superconductivity in a plethora of elements, and drives the formation of phases containing structural motifs whose atomic vibrations can be strongly coupled to the underlying electronic structure. From the clathrate-like LaH₁₀ to the covalent H₃S – and the intensely-discussed CSH room-temperature superconductor – the playing field of high-pressure materials is a promising one for the future.

Acknowledgments

We acknowledge the NSF (DMR-1827815) for financial support. This material is based upon work supported by the U.S. Department of Energy, Office of Science, Fusion Energy Sciences under Award Number DE-SC0020340 to E.Z. K.P.H. thanks the US Department of Energy, National Nuclear Security Administration, through the Chicago-DOE Alliance Center under Cooperative Agreement Grant No. DE-NA0003975 for financial support. We thank Giacomo Scilla for his help in editing and preparing the manuscript.

References

- [1] Guillot, T.: The Interiors of Giant Planets: Models and Outstanding Questions. *Annu. Rev. Earth Planet Sci.* **33**, 493–530 (2005)
- [2] Zaghoo, M., Silvera, I.F.: Conductivity and dissociation in liquid metallic hydrogen and implications for planetary interiors. *Proc. Natl. Acad. Sci. USA* **114**(45), 11873–11877 (2017)
- [3] Matsuoka, T., Shimizu, K.: Direct observation of a pressure-induced metal-to-semiconductor transition in lithium. *Nature* **458**(7235), 186–189 (2009)
- [4] Ma, Y., Eremets, M., Oganov, A.R., Xie, Y., Trojan, I., Medvedev, S., Lyakhov, A.O., Valle, M., Prakapenka, V.: Transparent dense sodium. *Nature* **458**(7235), 182–185 (2009)
- [5] Polsin, D.N., Lazicki, A., Gong, X., Burns, S.J., Coppari, F., Hansen, L.E., Henderson, B.J., Huff, M.F., McMahon, M.I., Millot, M., Paul, R., Smith, R.F., Eggert, J.H., Collins, G.W., Rygg, J.R.: Structural complexity in ramp-compressed sodium to 480 GPa. *Nat. Commun.* **13**, 2354 (2022)
- [6] Bukowinski, M.S.T.: The Effect of Pressure on the Physics and Chemistry of Potassium. *Geophys. Res. Lett.* **3**, 491–494 (1976)
- [7] Atou, T., Hasegawa, M., Parker, L.J., Badding, J.V.: Unusual Chemical Behavior for Potassium under Pressure: Potassium-Silver Compounds. *J. Am. Chem. Soc.* **118**, 12104–12108 (1996)
- [8] Parker, L.J., Atou, T., Badding, J.V.: Transition Element-Like Chemistry for Potassium Under Pressure. *Science* **273**, 95–97 (1996)
- [9] Zhang, W., Oganov, A.R., Goncharov, A.F., Zhu, Q., Boulfelfel, S.E., Lyakhov, A.O., Stavrou, E., Somayazulu, M., Prakapenka, V.B., Konôpková, Z.: Unexpected stable stoichiometries of sodium chlorides. *Science* **342**(6165), 1502–1505 (2013)

- [10] Dong, X., Oganov, A.R., Goncharov, A.F., Stavrou, E., Lobanov, S., Saleh, G., Qian, G.-R., Zhu, Q., Gatti, C., Deringer, V.L., Dronskowski, R., Zhou, X.-F., Prakapenka, V.B., Konôpková, Z., Popov, I.A., Boldyrev, A.I., Wang, H.-T.: A stable compound of helium and sodium at high pressure. *Nature Chem.* **9**, 440–445 (2017)
- [11] Geballe, Z.M., Liu, H., Mishra, A.K., Ahart, M., Somayazulu, M., Meng, Y., Baldini, M., Hemley, R.J.: Synthesis and stability of lanthanum superhydrides. *Angew. Chem. Int. Ed.* **57**(3), 688 (2018)
- [12] Prewitt, C.T., Downs, R.T.: High-pressure crystal chemistry. *Rev. Mineral* **37**, 283–318 (1998)
- [13] Grochala, W., Hoffmann, R., Feng, J., Ashcroft, N.W.: The chemical imagination at work in *very* tight places. *Angew. Chem. Int. Ed.* **46**(20), 3620–3642 (2007)
- [14] Zhang, L., Wang, Y., Lv, J., Ma, Y.: Materials discovery at high pressures. *Nature Rev. Mater.* **2**, 17005 (2017)
- [15] Jayaraman, A.: Diamond anvil cell and high-pressure physical investigations. *Rev. Mod. Phys.* **55**, 65–108 (1983)
- [16] Bassett, W.A.: Diamond anvil cell, 50th birthday. *High Press. Res.* **29**, 163–186 (2009)
- [17] Li, B., Ji, C., Yang, W., Wang, J., Yang, K., Xu, R., Liu, W., Cai, Z., Chen, J., Mao, H.-k.: Diamond anvil cell behavior up to 4 Mbar. *Proc. Natl. Acad. Sci. USA* **115**, 1713–1717 (2018)
- [18] Dubrovinsky, L., Dubrovinskaia, N., Prakapenka, V.B., Abakumov, A.M.: Implementation of micro-ball nanodiamond anvils for high-pressure studies above 6 Mbar. *Nature Comm.* **3**, 1163 (2012)
- [19] Dubrovinskaia, N., Dubrovinsky, L., Solopova, N.A., Abakumov, A., Turner, S., Hanfland, M., Bykova, E., Bykov, M., Prescher, C., Prakapenka, V.B., Petitgirard, S., Chuvashova, I., Gasharova, B., Mathis, Y.-L., Ershov, P., Snigireva, I., Snigirev, A.: Terapascal static pressure generation with ultrahigh yield strength nanodiamond. *Sci. Adv.* **2**, 1600341 (2016)
- [20] Dewaele, A., Loubeyre, P., Occelli, F., Marie, O., Mezouar, M.: Toroidal diamond anvil cell for detailed measurements under extreme static pressures. *Nature Comm.* **9**, 2913 (2018)
- [21] Jenei, Z., O’Bannon, E.F., Weir, S.T., Cynn, H., Lipp, M.J., Evans, W.J.: Single crystal toroidal diamond anvils for high pressure experiments

- beyond 5 megabar. *Nature Comm.* **9**, 3563 (2018)
- [22] Duffy, T.S., Smith, R.F.: Ultra-High Pressure Dynamic Compression of Geological Materials. *Front. Earth. Sci.* **7**, 1–20 (2019)
- [23] Hansen, L.E., Fratanduono, D.E., Zhang, S., Hicks, D.G., Suer, T., Sprowal, Z.K., Huff, M.F., Gong, X., Henderson, B.J., Polsin, D.N., Zaghoo, M., Hu, S.X., Collins, G.W., Rygg, J.R.: Melting of magnesium oxide up to two terapascals using double-shock compression. *Phys. Rev. B* **104**, 014106 (2021)
- [24] Fratanduono, D.E., Millot, M., Braun, D.G., Ali, S.J., Fernandez-Pañella, A., Seagle, C.T., Davis, J.-P., Brown, J.L., Akahama, Y., Kraus, R.G., Marshall, M.C., Smith, R.F., O'Bannon, E.F., McNaney, J.M., Eggert, J.H.: Establishing gold and platinum standards to 1 terapascal using shockless compression. *Science* **372**, 1063–1068 (2021)
- [25] Smith, R.F., Eggert, J.H., Jeanloz, R., Duffy, T.S., Braun, D.G., Patterson, J.R., Rudd, R.E., Biener, J., Lazicki, A.E., Hamza, A.V., Wang, J., Braun, T., Benedict, L.X., Celliers, P.M., Collins, G.W.: Ramp compression of diamond to five terapascals. *Nature* **511**, 330–333 (2014)
- [26] Kraus, R.G., Hemley, R.J., Ali, S.J., Belof, J.L., Benedict, L.X., Bernier, J., Braun, D., Cohen, R.E., Collins, G.W., Coppari, F., Desjarlais, M.P., Fratanduono, D., Hamel, S., Krygier, A., Lazicki, A., McNaney, J., Millot, M., Myint, P.C., Newman, M.G., Rygg, J.R., Sterbentz, D.M., Stewart, S.T., Stixrude, L., Swift, D.C., Wehrenberg, C., Eggert, J.H.: Measuring the melting curve of iron at super-Earth core conditions. *Science* **375**(6577), 202–205 (2022)
- [27] Zurek, E., Grochala, W.: Predicting crystal structures and properties of matter under extreme conditions via quantum mechanics: the pressure is on. *Phys. Chem. Chem. Phys.* **17**, 2917–2934 (2015)
- [28] Pickard, C.J., Needs, R.J.: Structures at high pressure from random searching. *Phys. Status Solidi B* **246**(3), 536–540 (2009)
- [29] Oganov, A.R., Lyakhov, A.O., Valle, M.: How Evolutionary Crystal Structure Prediction Works – and Why. *Acc. Chem. Res.* **44**(3), 227–237 (2011)
- [30] Wang, Y., Ma, Y.: Perspective: Crystal structure prediction at high pressures. *J. Chem. Phys.* **140**(4), 040901 (2014)
- [31] Oganov, A.R., Chen, J., Gatti, C., Ma, Y., Ma, Y., Glass, C.W., Liu, Z., Yu, T., Kurakevych, O.O.O., Solozhenko, V.L.: Ionic high-pressure form of elemental boron. *Nature* **457**, 863–867 (2009)

- [32] Zhang, M., Liu, H., Li, Q., Gao, B., Wang, Y., Li, H., Chen, C., Ma, Y.: Superhard BC₃ in Cubic Diamond Structure. *Phys. Rev. Lett.* **114**, 015502 (2015)
- [33] Avery, P., Wang, X., Oses, C., Gossett, E., Proserpio, D.M., Toher, C., Curtarolo, S., Zurek, E.: Predicting superhard materials via a machine learning informed evolutionary structure search. *npj Comput. Mater.* **5**, 89 (2019)
- [34] Liu, H., Naumov, I.I., Hoffmann, R., Ashcroft, N.W., Hemley, R.J.: Potential high- T_c superconducting lanthanum and yttrium hydrides at high pressure. *Proc. Natl. Acad. Sci. U.S.A.* **114**, 6990–6995 (2017)
- [35] Peng, F., Sun, Y., Pickard, C.J., Needs, R.J., Wu, Q., Ma, Y.: Hydrogen clathrate structures in rare earth hydrides at high pressures: possible route to room-temperature superconductivity. *Phys. Rev. Lett.* **119**, 107001 (2017)
- [36] Kruglov, I.A., Kvashnin, A.G., Goncharov, A.F., Oganov, A.R., Lobanov, S.S., Holtgrewe, N., Jiang, S., Prakapenka, V.B., Greenberg, E., Yanilkin, A.V.: Uranium polyhydrides at moderate pressures: Prediction, synthesis, and expected superconductivity. *Sci. Adv.* **4**, 9776 (2009)
- [37] Drozdov, A.P., Kong, P.P., Minkov, V.S., Besedin, S.P., Kuzovnikov, M.A., Mozaffari, S., Balicas, L., Balakirev, F.F., Graf, D.E., Prakapenka, V.B., Greenberg, E., Knyazev, D.A., Tkacz, M., Eremets, M.I.: Superconductivity at 250 K in lanthanum hydride under high pressures. *Nature* **569**(7757), 528–531 (2019)
- [38] Semenov, D.V., Troyan, I.A., Ivanova, A.G., Kvashnin, A.G., Kruglov, I.A., Hanfland, M., Sadakov, A.V., Sobolevskiy, O.A., Pervakov, K.S., Lyubutin, I.S., Glazyrin, K.V., Giordano, N., Karimov, D.N., Vasiliev, A.L., Akashi, R., Pudalov, V.M., Oganov, A.R.: Superconductivity at 253 K in lanthanum-yttrium ternary hydrides. *Mater. Today* **48**, 18–28 (2021)
- [39] Pickett, W., Eremets, M., Heil, C., Hemley, R., Pierleoni, C., Dias, R., Amsler, M., Ma, Y., Kolmogorov, A., Oganov, A., Pickard, C.J., Bi, T., Gross, H., Errea, I., Arita, R., Margine, R., Gonnelli, R., Valenti, R., Xie, S., Boeri, L., Hirschfeld, P., Hennig, R., Profeta, G., Sanna, A., Zurek, E.: The 2021 room-temperature superconductivity roadmap. *J. Phys. Condens. Mat.* **34**, 183002 (2022). <https://doi.org/10.1088/1361-648x/ac2864>
- [40] Dye, J.L.: Electrides: Early Examples of Quantum Confinement. *Acc. Chem. Res.* **42**, 1564–1572 (2009)

- [41] Zurek, E.: Alkali Metals in Ethylenediamine: A Computational Study of the Optical Absorption Spectra and NMR Parameters of $[M(en)_3^+ \cdot M^-]$ Ion-Pairs. *J. Am. Chem. Soc.* **133**, 4829–4839 (2011)
- [42] Riedel, R., Seel, A.G., Malko, D., Miller, D.P., Sperling, B.T., Choi, H., Headen, T.F., Zurek, E., Porch, A., Kucernak, A., Pyper, N.C., Edwards, P.P., Barrett, A.G.M.: Superalkali-Alkalide Interactions and Ion Pairing in Low-Polarity Solvents. *J. Am. Chem. Soc.* **143**, 3934–3943 (2021)
- [43] Abella, L., Philips, A., Autschbach, J.: *Ab initio* molecular dynamics study of sodium NMR chemical shifts in the methylamine solution of $[\text{Na}^+[\text{2.2.2}]\text{cryptand Na}^-]$. *Phys. Chem. Chem. Phys.* **23**, 339–346 (2021)
- [44] Botana, J., Miao, M.-S.: Pressure-stabilized lithium caesides with caesium anions beyond the -1 state. *Nat. Commun.* **5**(1), 1–8 (2014)
- [45] Pauling, L.: The Nature of the Chemical Bond. IV. The Energy of Single Bonds and the Relative Electronegativity of Atoms. *J. Am. Chem. Soc.* **54**, 3570–3582 (1932)
- [46] Pearson, R.G.: Absolute electronegativity and absolute hardness of Lewis acids and bases. *J. Am. Chem. Soc.* **107**, 6801–6806 (1985)
- [47] Mulliken, R.S.: A New Electroaffinity Scale; Together with Data on Valence States and on Valence Ionization Potentials and Electron Affinities. *J. Chem. Phys.* **2**, 782–793 (1934)
- [48] Dong, X., Oganov, A.R., Cui, H., Zhou, X.-F., Wang, H.-T.: Electronegativity and chemical hardness of elements under pressure. *Proc. Natl. Acad. Sci.* **119**, 2117416119 (2022)
- [49] Allen, L.C.: Electronegativity Is the Average One-Electron Energy of the Valence-Shell Electrons in Ground-State Free Atoms. *J. Am. Chem. Soc.* **111**, 9003–9014 (1989)
- [50] Rahm, M., Zeng, T., Hoffmann, R.: Electronegativity Seen as the Ground-State Average Valence Electron Binding Energy. *J. Am. Chem. Soc.* **141**, 342–351 (2019). <https://doi.org/10.1021/jacs.8b10246>
- [51] Rahm, M., Erhart, P., Cammi, R.: Relating atomic energy, radius, and electronegativity through compression. *Chem. Sci.* **12**, 2397–2403 (2021)
- [52] Racioppi, S., Rahm, M.: In-Situ Electronegativity and the Bridging of Chemical Bonding Concepts. *Chem. Eur. J.* **27**, 18156–18167 (2021)
- [53] Sternheimer, R.: On the Compressibility of Metallic Cesium. *Phys. Rev.*

- 78**, 235–243 (1950)
- [54] Louie, S.G., Cohen, M.L.: Electronic structure of cesium under pressure. *Phys. Rev. B* **10**, 3237–3245 (1974)
- [55] Takemura, K., Minomura, S., Shimomura, O.: X-Ray Diffraction Study of Electronic Transitions in Cesium under High Pressure. *Phys. Rev. Lett.* **49**, 1772–1775 (1982)
- [56] Connerade, J.P., Semaoune, R.: Atomic compressibility and reversible insertion of atoms into solids. *J. Phys. B: At. Mol. Opt. Phys.* **33**, 3467–3484 (2000)
- [57] Rahm, M., Cammi, R., Ashcroft, N.W., Hoffmann, R.: Squeezing All Elements in the Periodic Table: Electron Configuration and Electronegativity of the Atoms under Compression. *J. Am. Chem. Soc.* **141**, 10253–10271 (2019)
- [58] Zurek, E., Jepsen, O., Andersen, O.K.: Muffin-Tin Orbital Wannier-Like Functions for Insulators and Metals. *ChemPhysChem* **6**, 1934–1942 (2005)
- [59] Neaton, J.B., Ashcroft, N.W.: Pairing in dense lithium. *Nature* **400**, 141–144 (1999)
- [60] Hanfland, M., Syassen, J., Christensen, N.E., Novikov, D.L.: New high-pressure phases of lithium. *Nature* **408**, 174–178 (2000)
- [61] Naumov, I.I., Hemley, R.J., Hoffmann, R., Ashcroft, N.W.: Chemical bonding in hydrogen and lithium under pressure. *J. Chem. Phys.* **143**, 064702 (2015)
- [62] Degtyareva, V.F.: Potassium under pressure: Electronic origin of complex structures. *Solid State Sci.* **36**, 62–72 (2014)
- [63] Takemura, K., Christensen, N.E., Novikov, D.L., Syassen, K., Schwarz, U., Hanfland, M.: Phase stability of highly compressed cesium. *Phys. Rev. B* **61**, 14399–14404 (2000)
- [64] McMahan, A.K.: Alkali-metal structures above the *s-d* transition. *Phys. Rev. B* **29**, 5982–5985 (1984)
- [65] McMahan, M.I., Nelmes, R.J., Schwarz, U., Syassen, K.: Composite incommensurate K-III and a commensurate form: Study of a high-pressure phase of potassium. *Phys. Rev. B* **74**, 140102 (2006)
- [66] Hooper, J., Zurek, E.: High pressure potassium polyhydrides: a chemical perspective. *J. Phys. Chem. C* **116**(24), 13322–13328 (2012)

- [67] Dewaele, A., Pepin, C.M., Geneste, G., Garbarino, G.: Reaction between nickel or iron and xenon under high pressure. *High Pressure Research* **37**, 137–146 (2017)
- [68] Stavrou, E., Yao, Y., Goncharov, A.F., Lobanov, S.S., Zaug, J.M., Liu, H., Greenberg, E., Prakapenka, V.B.: Synthesis of Xenon and Iron-Nickel Intermetallic Compounds at Earth’s Core Thermodynamic Conditions. *Phys. Rev. Lett.* **120**, 096001 (2018)
- [69] Snider, E., Dasenbrock-Gammon, N., McBride, R., Wang, X., Meyers, N., Lawler, K.V., Zurek, E., Salamat, A., Dias, R.P.: Synthesis of Yttrium Superhydride Superconductor with a Transition Temperature up to 262 K by Catalytic Hydrogenation at High Pressures. *Phys. Rev. Lett.* **126**, 117003 (2021)
- [70] Somayazulu, M., Ahart, M., Mishra, A.K., Geballe, Z.M., Baldini, M., Meng, Y., Struzhkin, V.V., Hemley, R.J.: Evidence for Superconductivity above 260 K in Lanthanum Superhydride at Megabar Pressures. *Phys. Rev. Lett.* **122**, 027001 (2019)
- [71] Ma, L., Wang, K., Xie, Y., Yang, X., Wang, Y., Zhou, M., Liu, H., Yu, X., Zhao, Y., Wang, H., Liu, G., Ma, Y.: High-temperature superconducting phase in clathrate calcium hydride CaH₆ up to 215 K at a pressure of 172 GPa. *Phys. Rev. Lett.* **128**, 167001 (2022)
- [72] Li, Z., Zhang, C., Wang, X., Zhang, S., Jia, Y., Feng, S., Lu, K., Zhao, J., Zhang, J., Min, B., Long, Y., Yu, R., Wang, L., Ye, M., Zhang, Z., Prakapenka, V., Chariton, S., Ginsberg, P.A., Bass, J., Yuan, S., Liu, H., Jin, C.: Superconductivity above 200 K discovered in superhydrides of calcium. *Nature Commun.* **13**, 2863 (2022)
- [73] Wang, H., John, S.T., Tanaka, K., Iitaka, T., Ma, Y.: Superconductive sodalite-like clathrate calcium hydride at high pressures. *Proc. Natl. Acad. Sci. USA* **109**(17), 6463–6466 (2012)
- [74] Dye, J.L.: Compounds of Alkali Metal Anions. *Angew. Chem. Int. Ed.* **18**, 587–598 (1979)
- [75] Pickard, C.J., Needs, R.J.: Predicted Pressure-Induced s-Band Ferromagnetism in Alkali Metals. *Phys. Rev. Lett.* **107**, 087201 (2011)
- [76] Hasegawa, M., Atou, T., Badding, J.V.: High-Pressure Synthesis of an Alkali Metal-Transition metal Laves Phase: KAg₂. *J. Solid State Chem.* **130**, 311–315 (1997)
- [77] Lee, K.K.M., Jeanloz, R.: High-pressure alloying of potassium and iron: Radioactivity in the Earth’s core? *Geophys. Res. Lett.* **30** (2003)

- [78] Adeleke, A.A., Stavrou, E., Adeniyi, A.O., Wan, B., Gou, H., Yao, Y.: Two good metals make a semiconductor: A potassium-nickel compound under pressure. *Phys. Rev. B* **102**, 134120 (2020)
- [79] Brgoch, J., Hermus, M.: Pressure-Stabilized Ir³⁻ in a Superconducting Potassium Iridide. *J. Phys. Chem. C* **120**, 20033–20039 (2016)
- [80] Lotfi, S., Brgoch, J.: Predicting pressure-stabilized alkali metal iridides: A-Ir (A=Rb, Cs). *Comput. Mater. Sci.* **158**, 124–129 (2019)
- [81] Yang, G., Yang, Y., Peng, F., Bergara, A., Ma, Y.: Gold as a 6p-Element in Dense Lithium Aurides. *J. Am. Chem. Soc.* **138**, 4046–4052 (2016)
- [82] Botana, J., Wang, X., Hou, C., Yan, D., Lin, H., Ma, Y., Miao, M.: Mercury under Pressure acts as a Transition Metal: Calculated from First Principles. *Angew. Chem. Int. Ed.* **54**, 9280–9283 (2015)
- [83] Savin, A.: The Electron Localization Function (ELF) and Its Relatives: Interpretations and Difficulties. *J. Mol. Struct.-Theochem.* **727**(1-3), 127–131 (2005)
- [84] Miao, M.-s.: Caesium in high oxidation states and as a p-block element. *Nat. Chem.* **5**(10), 846–852 (2013)
- [85] Liu, C., Nikolaev, S.A., Wen, R., Burton, L.A.: Electrides: a review. *J. Mater. Chem. C* **8**, 10551–10567 (2020)
- [86] Zurek, E., Edwards, P.P., Hoffmann, R.: A Molecular Perspective on Lithium-Ammonia Solutions. *Angew. Chem. Int. Ed.* **48**, 8198–8232 (2009)
- [87] Miao, M., Hoffmann, R.: High-Pressure Electrides: The Chemical Nature of Interstitial Quasiatoms. *J. Am. Chem. Soc.* **137**, 3631–3637 (2015)
- [88] Neaton, J.B., Ashcroft, N.W.: On the constitution of sodium at higher densities. *Phys. Rev. Lett.* **86**, 2830–2833 (2001)
- [89] Li, P., Gao, G., Wang, Y., Ma, Y.: Crystal Structures and Exotic Behavior of Magnesium under Pressure. *J. Phys. Chem. C* **114**, 21745–21749 (2010)
- [90] Dong, X., Oganov, A.R.: Electrides and Their High-Pressure Chemistry. In: *Correlations in Condensed Matter Under Extreme Conditions*, pp. 69–84. Springer, Cham (2017). Chap. 6
- [91] Modak, P., Verma, A.K.: Pressure induced multi-centre bonding and metal-insulator transition in PtAl₂. *Phys. Chem. Chem. Phys.* **21**, 13337–13346 (2019)

- [92] Miao, M.-S., Hoffmann, R.: High pressure electrides: A predictive chemical and physical theory. *Acc. Chem. Res.* **47**(4), 1311–1317 (2014)
- [93] Wang, B., Hilleke, K.P., Wang, X., Polsin, D.N., Zurek, E.: Topological Electride Phase of Sodium at High Pressures and Temperatures. *arXiv* (2022). <https://doi.org/10.48550/ARXIV.2205.06251>. <https://arxiv.org/abs/2205.06251>
- [94] Li, Y., Wang, Y., Pickard, C.J., Needs, R.J., Wang, Y., Ma, Y.: Metallic Icosahedron Phase of Sodium at Terapascal Pressures. *Phys. Rev. Lett.* **114**, 125501 (2015)
- [95] Vegas, A., Grzechnik, A., Hanfland, M., Mühle, C., Jansen, M.: Antifluorite to Ni₂In-type phase transition in K₂S at high pressures. *Solid State Sci.* **4**, 1077–1081 (2002)
- [96] Santamaria-Perez, D., Vegas, A., Muehle, C., Jansen, M.: High-pressure experimental study on Rb₂S: antifluorite to Ni₂In-type phase transitions. *Acta Crystallogr. B* **67**, 109–115 (2011)
- [97] Marques, M., Ackland, G.J., Lundegaard, L.F., Stinton, G., Nelmes, R.J., McMahon, M.I., Contreras-Garcia, J.: Potassium under pressure: A Pseudobinary Ionic Compound. *Phys. Rev. Lett.* **103**, 115501 (2009)
- [98] McMahon, M.I., Gregoryanz, E., Lundegaard, L.F., Loa, I., Guillaume, C., Nelmes, R.J., Kleppe, A.K., Amboage, M., Wilhelm, H., Jephcoat, A.P.: Structure of sodium above 100 GPa by single-crystal x-ray diffraction. *Proc. Natl. Acad. Sci.* **104**, 17297–17299 (2007)
- [99] Guillaume, C.L., Gregoryanz, E., Degtyareva, O., McMahon, M.I., Hanfland, M., Evans, S., Guthrie, M., Sinogeikin, S.V., Mao, H.-k.: Cold melting and solid structures of dense lithium. *Nature Phys.* **7**, 211–214 (2011)
- [100] Miao, M., Hoffmann, R., Botana, J., Naumov, I.I., Hemley, R.J.: Quasi-molecules in Compressed Lithium. *Angew. Chem. Int. Ed.* **56**, 972–975 (2017)
- [101] Dronskowski, R., Blöchl, P.E.: Crystal Orbital Hamilton Populations (COHP). Energy-Resolved Visualization of Chemical Bonding in Solids Based on Density-Functional Calculations. *J. Phys. Chem.* **97**, 8617–8624 (1993)
- [102] Miao, M.-s., Wang, X., Brgoch, J., Spera, F., Jackson, M.G., Kresse, G., Lin, H.: Anionic chemistry of noble gases: formation of Mg–NG (NG= Xe, Kr, Ar) compounds under pressure. *J. Am. Chem. Soc.* **137**(44), 14122–14128 (2015)

- [103] Botana, J., Brgoch, J., Hou, C., Miao, M.: Iodine Anions beyond -1: Formation of Li_nI ($n=2-5$) and Its Interaction with Quasiatoms. *Inorg. Chem.* **55**, 9377–9382 (2016)
- [104] Miao, M., Sun, Y., Zurek, E., Lin, H.: Chemistry under high pressure. *Nat. Rev. Chem.* **4**, 508–527 (2020)
- [105] Pauling, L.: Principles determining the structure of high-pressure metals: The structures of cesium(IV) and cesium(V). *Proc. Natl. Acad. Sci. USA* **86**, 1431–1433 (1989)
- [106] von Schnering, H.G., Nesper, R.: How Nature Adapts Chemical Structures to Curved Surfaces. *Angew. Chem. Int. Ed.* **26**, 1059–1080 (1987)
- [107] Olijnyk, H., Holzapfel, W.B.: Phase transitions in K and Rb under pressure. *Phys. Lett. A* **99**, 381–383 (1983)
- [108] Ma, Y., Oganov, A.R., Xie, Y.: High-pressure structures of lithium, potassium, and rubidium predicted by an *ab initio* evolutionary algorithm. *Phys. Rev. B* **78**, 014102 (2008)
- [109] Lundegaard, L.F., Marques, M., Stinton, G., Ackland, G.J., Nelmes, R.J., McMahan, M.I.: Observation of the *oP8* crystal structure in potassium at high pressure. *Phys. Rev. B* **80**, 020101 (2009)
- [110] Schwarz, U., Grzechnik, A., Syassen, K., Loa, I., Hanfland, M.: Rubidium-IV: A High Pressure Phase with Complex Crystal Structure. *Phys. Rev. Lett.* **83**, 4085–4088 (1999)
- [111] McMahan, M.I., Rekhi, S., Nelmes, R.J.: Pressure Dependent Incommensuration in Rb-IV. *Phys. Rev. Lett.* **87**, 055501 (2001)
- [112] McMahan, M.I., Nelmes, R.J.: High-pressure structures and phase transformations in elemental metals. *Chem. Soc. Rev.* **35**, 943–963 (2006)
- [113] Gregoryanz, E., Lundegaard, L.F., McMahan, M.I., Guillaume, C., Nelmes, R.J., Mezouar, M.: Structural Diversity of Sodium. *Science* **320**, 1054–1057 (2008)
- [114] Woolman, G., Robinson, V.N., Marques, M., Loa, I., Ackland, G.J., Hermann, A.: Structural and electronic properties of the alkali metal incommensurate phases. *Phys. Rev. Mater.* **2**, 053604 (2018)
- [115] Zhou, Y., Xu, Q., Zhu, C., Li, Q., Liu, H., Wang, H., Tse, J.S.: Predicted lithium-iron compounds under high pressure. *RSC Adv.* **6**, 66721–66728

(2016)

- [116] Zhou, Y., Wang, H., Zhu, C., Liu, H., Tse, J.S., Ma, Y.: Prediction of Host-Guest Na-Fe Intermetallics at High Pressure. *Inorg. Chem.* **55**, 7026–7032 (2016)
- [117] Zhang, J., Chen, G., Liu, H.: Stable Structures and Superconductivity in a Y-Si System under High Pressure. *J. Phys. Chem. Lett.* **12**, 10388–10393 (2021)
- [118] Pepin, R.O., Porcelli, D.: Origin of Noble Gases in the Terrestrial Planets. *Rev. Mineral. Geochem.* **47**, 191–246 (2002)
- [119] Shcheka, S.S., Keppler, H.: The origin of the terrestrial noble-gas signature. *Nature* **490**, 531–534 (2012)
- [120] Marty, B.: The origins and concentrations of water, carbon, nitrogen, and noble gases on Earth. *Earth & Planet. Sci. Lett.* **313–314**, 56–66 (2012)
- [121] Caldwell, W.A., Nguyen, J.H., Pfrommer, B.G., Mauri, F., Louie, S.G., Jeanloz, R.: Structure, Bonding, and Geochemistry of Xenon at High Pressures. *Science* **277**, 930–933 (2012)
- [122] Lee, K.K.M., Steinle-Neumann, G.: High-pressure alloying of iron and xenon: “Missing” Xe in the Earth’s core? *J. Geophys. Res.* **111**, 02202 (2006)
- [123] Zhu, L., Liu, H., Pickard, C.J., Zou, G., Ma, Y.: Reactions of xenon with iron and nickel are predicted in the Earth’s inner core. *Nat. Chem.* **6**(7), 644–648 (2014)
- [124] Peng, F., Song, X., Liu, C., Li, Q., Miao, M., Chen, C., Ma, Y.: Xenon iron oxides predicted as potential Xe hosts in Earth’s lower mantle. *Nat. Commun.* **11**(1), 1–7 (2020)
- [125] Adeleke, A.A., Kunz, M., Greenberg, E., Prakapenka, V.B., Yao, Y., Stavrou, E.: A High-Pressure Compound of Argon and Nickel: Noble Gas in the Earth’s Core? *ACS Earth Space Chem.* **3**, 2517–2524 (2019)
- [126] Zhu, Q., Jung, D.Y., Oganov, A.R., Glass, C.W., Gatti, C., Lyakhov, A.O.: Stability of xenon oxides at high pressures. *Nat. Chem.* **5**(1), 61–65 (2013)
- [127] Hermann, A., Schwerdtfeger, P.: Xenon suboxides stable under pressure. *J. Phys. Chem. Lett.* **5**(24), 4336–4342 (2014)
- [128] Dewaele, A., Worth, N., Pickard, C.J., Needs, R.J., Pascarelli, S.,

- Mathon, O., Mezouar, M., Irifune, T.: Synthesis and stability of xenon oxides Xe_2O_5 and Xe_3O_2 under pressure. *Nature Chem.* **8**, 784–790 (2016)
- [129] Zaleski-Ejgierd, P., Lata, P.M.: Krypton oxides under pressure. *Sci. Rep.* **6**, 18938 (2016)
- [130] Peng, F., Wang, Y., Wang, H., Zhang, Y., Ma, Y.: Stable xenon nitride at high pressures. *Phys. Rev. B* **92**(9), 094104 (2015)
- [131] Howie, R.T., Turnbull, R., Binns, J., Frost, M., Dalladay-Simpson, P., Gregoryanz, E.: Formation of xenon-nitrogen compounds at high pressure. *Sci. Rep.* **6**, 34896 (2016)
- [132] Bovornratanaraks, T., Tsuppayakorn-ae, P., Luo, W., Ahuja, R.: Ground-state structure of semiconducting and superconducting phases in xenon carbides at high pressure. *Sci. Rep.* **9**, 2459 (2019)
- [133] Kurzydłowski, D., Zaleski-Ejgierd, P.: Ground-state structure of semiconducting and superconducting phases in xenon carbides at high pressure. *Phys. Chem. Chem. Phys.* **18**, 2309–2313 (2016)
- [134] Kurzydłowski, D., Sołtysiak, M., Džoleva, A., Zaleski-Ejgierd, P.: High-Pressure Reactivity of Kr and F_2 -Stabilization of Krypton in the +4 Oxidation State. *Crystals* **7**, 329 (2017)
- [135] Peng, F., Botana, J., Wang, Y., Ma, Y., Miao, M.: Unexpected Trend in Stability of Xe-F Compounds under Pressure Driven by Xe-Xe Covalent Bonds. *J. Phys. Chem. Lett.* **7**, 4562–4567 (2016)
- [136] Zarifi, N., Liu, H., Tse, J.S., Zurek, E.: Crystal Structures and Electronic Properties of Xe-Cl Compounds at High Pressure. *J. Phys. Chem. C* **122**, 2941–2950 (2018)
- [137] Li, X., Hermann, A., Peng, F., Lv, J., Wang, Y., Wang, H., Ma, Y.: Stable Lithium Argon compounds under high pressure. *Sci. Rep.* **5**, 16675 (2015)
- [138] Liu, Z., Botana, J., Miao, M., Yan, D.: Unexpected Xe anions in XeLi_n intermetallic compounds. *EPL* **117**, 26002 (2017)
- [139] Zhang, S., Bi, H., Wei, S., Wang, J., Li, Q., Ma, Y.: Crystal Structures and Electronic Properties of Cesium Xenides at High Pressures. *J. Phys. Chem. C* **119**, 24996–25002 (2015)
- [140] Sanloup, C., Bonev, S.A., Hochlaf, M., Maynard-Casely, H.E.: Reactivity of xenon with ice at planetary conditions. *Phys. Rev. Lett.* **110**(26),

- 265501 (2013)
- [141] Monserrat, R., Martinez-Canales, M., Needs, R.J., Pickard, C.J.: Helium-Iron Compounds at Terapascal Pressures. *Phys. Rev. Lett.* **121**, 015301 (2018)
- [142] Liu, C., Gao, H., Hermann, A., Wang, Y., Miao, M., Pickard, C.J., Needs, R.J., Wang, H.-T., Xing, D., Sun, J.: Plastic and Superionic Helium Ammonia Compounds under High Pressure and High Temperature. *Phys. Rev. X* **10**, 021007 (2020)
- [143] Liu, C., Yao, Y., Klug, D.D.: Stable structures of He and H₂O at high pressure. *Phys. Rev. B* **91**, 014102 (2015)
- [144] Liu, C., Gao, H., Wang, Y., Needs, R.J., Pickard, C.J., Sun, J., Wang, H.-T., Xing, D.: Multiple superionic states in helium-water compounds. *Nat. Phys.* **15**, 1065–1070 (2019)
- [145] Vos, W.L., Finger, L.W., Hemley, R.J., Hu, J.Z., Mao, H.K., Schouten, J.A.: A high-pressure van der Waals compound in solid nitrogen-helium mixtures. *Nature* **358**, 46–48 (1992)
- [146] Li, Y., Feng, X., Liu, H., Hao, J., Redfern, S.A.T., Lei, W., Liu, D., Ma, Y.: Route to high-energy density polymeric nitrogen *t*-N via He-N compounds. *Nat. Commun.* **9**, 722 (2018)
- [147] Wang, Y., Zhang, J., Liu, H., Yang, G.: Prediction of the Xe-He binary phase diagram at high pressures. *Chem. Phys. Lett.* **640**, 115–118 (2015)
- [148] Cazorla, C., Errandonea, D., Sola, E.: High-pressure phases, vibrational properties, and electronic structure of Ne(He)₂ and Ar(He)₂: A first-principles study. *Phys. Rev. B* **80**, 064105 (2009)
- [149] Loubeyre, P., Jean-Louis, M., LeToullec, R., Charon-Gérard, L.: High pressure measurements of the He-Ne binary phase diagram at 296 K: Evidence for the stability of a stoichiometric Ne(He)₂ solid. *Phys. Rev. Lett.* **70**, 178–181 (1993)
- [150] Liu, Z., Botana, J., Hermann, A., Valdez, S., Zurek, E., Yan, D., Lin, H., Miao, M.: Reactivity of He with ionic compounds under high pressure. *Nature Comm.* **9**, 951 (2018)
- [151] Gao, H., Sun, J., Pickard, C.J., Needs, R.J.: Prediction of pressure-induced stabilization of noble-gas-atom compounds with alkali oxides and alkali sulfides. *Phys. Rev. Mater.* **3**, 015002 (2019)
- [152] Zhang, J., Lv, J., Li, H., Feng, X., Lu, C., Redfern, S.A.T., Liu, H.,

- Chen, C., Ma, Y.: Rare Helium-Bearing Compound FeO₂He Stabilized at Deep-Earth Conditions. *Phys. Rev. Lett.* **121**, 255703 (2018)
- [153] Hume-Rothery, W., Raynor, G.V.: The structure of metals and alloys, 4th edn. Institute of Metals, London (1962)
- [154] Miedema, A.R.: A simple model for alloys, I. Rules for the alloying behaviour of transition metals. *Philips Tech. Rev.* **33**, 149–160 (1973)
- [155] Miedema, A.R.: A simple model for alloys, II. The influence of ionicity on the stability and other physical properties of alloys. *Philips Tech. Rev.* **33**, 196–202 (1973)
- [156] Darken, L.S., Gurry, R.W.: Physical chemistry of metals. McGraw-Hill, New York (1953)
- [157] Chelikowsky, J.R.: Solid solubilities in divalent alloys. *Phys. Rev. B* **19**, 686–701 (1979)
- [158] Alonso, J.A., Simozar, S.: Prediction of solid solubility in alloys. *Phys. Rev. B* **22**, 5583–5589 (1980)
- [159] Wang, Z., Huang, Y., Yang, Y., Wang, J., Liu, C.T.: Atomic-size effect and solid solubility of multicomponent alloys. *Scr. Mater.* **94**, 28–31 (2015)
- [160] Dubrovinskaia, N., Dubrovinsky, L., McCammon, C.: Iron-magnesium alloying at high pressures and temperatures. *J. Phys. Condens. Matter* **16**, 1143 (2004)
- [161] Gao, P., Su, C., Shao, S., Wang, S., Liu, P., Liu, S., Lv, J.: Iron-magnesium compounds under high pressure. *New J. Chem.* **43**, 17403–17407 (2019)
- [162] Fang, Y., Sun, Y., Wang, R., Zheng, F., Wu, S., Wang, C.-Z., Wentzcovitch, R.M., Ho, K.-M.: Unconventional iron-magnesium compounds at terapascal pressures. *Phys. Rev. B* **104**, 144109 (2021)
- [163] Dubrovinskaia, N., Dubrovinsky, L., Kantor, I., Crichton, W.A., Dmitriev, V., Prakapenka, V., Shen, G., Vitos, L., Ahuja, R., Johansson, B., Abrikosov, I.A.: Beating the Miscibility Barrier between Iron Group Elements and Magnesium by High-Pressure Alloying. *Phys. Rev. Lett.* **95**, 245502 (2005)
- [164] Feng, J., Hennig, R.G., Ashcroft, N.W., Hoffmann, R.: Emergent reduction of electronic state dimension in dense ordered Li-Be alloys. *Nature* **451**, 445–448 (2008)

- [165] Degtyareva, V.F.: Simple metals at high pressures: the Fermi sphere-Brillouin zone interaction model. *Phys.-Usp.* **49**, 369–388 (2006)
- [166] Berger, R.F., Walters, P.L., Lee, S., Hoffmann, R.: Connecting the Chemical and Physical Viewpoints of What Determines Structure: From 1-D Chains to γ -Brasses. *Chem. Rev.* **111**, 4522–4545 (2011)
- [167] Feng, J., Hoffmann, R., Ashcroft, N.W.: Double-diamond NaAl via pressure: Understanding structure through Jones zone activation. *J. Chem. Phys.* **132**, 114106 (2010)
- [168] Guo, K., Akselrud, L., Bobnar, M., Burkhardt, U., Schmidt, M., Zhao, J.-T., Schwarz, U., Grin, Y.: Weak Interactions under Pressure: *hp*-CuBi and Its Analogues. *Angew. Chem. Int. Ed.* **56**, 5620–5624 (2017)
- [169] Clarke, S., Amsler, M., Walsh, J.P.S., Yu, T., Wang, Y., Meng, Y., Jacobsen, S., Wolverton, C., Freedman, D.E.: Creating binary Cu-Bi Compounds via High-Pressure Synthesis: A Combined Experimental and Theoretical Study. *Chem. Mater.* **29**, 5276–5285 (2017)
- [170] Chen, Y.L., Analytis, J.G., Chu, J.-H., Liu, Z.K., Mo, S.-K., Qi, X.L., Zhang, H.J., Lu, D.H., Dai, X., Fang, Z., Zhang, S.C., Fisher, I.R., Hussain, Z., Shen, Z.-X.: Experimental Realization of a Three-Dimensional Topological Insulator, Bi₂Te. *Science* **325**, 178–181 (2009)
- [171] Liu, Z.K., Zhou, B., Zhang, Y., Wang, Z.J., Weng, H.M., Prabhakaran, D., Mo, S.-K., Shen, Z.X., Fang, Z., Dai, X., Hussain, Z., Chen, Y.L.: Discovery of a Three-Dimensional Topological Dirac Semimetal, Na₃Bi. *Science* **343**, 864–867 (2014)
- [172] Reynolds, J.M., Lane, C.T.: Superconducting Bismuth Alloys. *Phys. Rev.* **79**, 405 (1950)
- [173] Matthias, B.T., A., J., Geballe, T.H., Andres, K., Corenzwit, E.: Many More Superconducting Bismuth Phases. *Phys. Rev. Lett.* **17**, 640–643 (1966)
- [174] Hor, Y.S., Williams, A.J., Checkelsky, J.G., Roushan, P., Seo, J., Xu, Q., Zandbergen, H.W., Yazdani, A., Ong, N.P., Cava, R.J.: Superconductivity in Cu_xBi₂Se₃ and its Implications for Pairing in the Undoped Topological Insulator. *Phys. Rev. Lett.* **104**, 057001 (2010)
- [175] Walsh, J.P.S., Clarke, S.M., Meng, Y., Jacobsen, S.D., Freedman, D.E.: Discovery of FeBi₂. *ACS Cent. Sci.* **6**, 867–871 (2016)
- [176] Amsler, M., Naghavi, S.S., Wolverton, C.: Prediction of superconducting iron-bismuth intermetallic compounds at high pressure. *Chem. Sci.* **8**,

- 2226 (2017)
- [177] Amsler, M., Hegde, V.I., Jacobsen, S.D., Wolverton, C.: Exploring the High-Pressure Materials Genome. *Phys. Rev. X* **8**, 041021 (2018)
- [178] Walsh, J.P.S., Clarke, S.M., Puggioni, D., Tamerius, A.D., Meng, Y., Rondinelli, J.M., Jacobsen, S.D., Freedman, D.E.: MnBi₂: A Metastable High-Pressure Phase in the Mn-Bi System. *Chem. Mater.* **31**, 3083–3088 (2019)
- [179] Takizawa, H., Uheda, K., Endo, T.: A new ferromagnetic polymorph of CrSb₂ synthesized under high pressure. *J. Alloys Compd.* **287**, 145–149 (1999)
- [180] Wu, X., Steinle-Neumann, G., Qin, S., Kanzaki, M., Dubrovinsky, L.: Pressure-induced phase transitions of AX₂-type iron pnictides: an *ab initio* study. *J. Phys.: Condens. Matter* **21**, 185403 (2009)
- [181] Poffo, C.M., Souza, S.M., Trichês, D.M., de Lima, J.C., Grandi, T.A., Polian, A., Gauthier, M.: Structural and optical studies of FeSb₂ under high pressure. *Physica B* **407**, 4686–4694 (2012)
- [182] Schwarz, U., Tence, S., Janson, O., Koz, C., Krellner, C., Burkhardt, U., Rosner, H., Steglich, F., Grin, Y.: CoBi₃: A Binary Cobalt-Bismuth Compound and Superconductor. *Angew. Chem. Int. Ed.* **52**, 9853–9857 (2013)
- [183] Tencé, S., Janson, O., Krellner, C., Rosner, H., Schwarz, U., Grin, Y., Steglich, F.: CoBi₃- the first binary compound of cobalt with bismuth: high-pressure synthesis and superconductivity. *J. Phys.: Condens. Matter* **26**, 395701 (2014)
- [184] Clarke, S.M., Walsh, J.P.S., Amsler, M., Malliakas, C.D., Yu, T., Goedecker, S., Wang, Y., Wolverton, C., Freedman, D.E.: Discovery of a Superconducting Cu-Bi Intermetallic Compound by High-Pressure Synthesis. *Angew. Chem. Int. Ed.* **128**, 13644–13647 (2016)
- [185] Amsler, M., Wolverton, C.: Dense superconducting phases of copper-bismuth at high pressure. *Phys. Rev. M* **1**, 031801 (2017)
- [186] Altman, A.B., Tamerius, A.D., Koocher, N.Z., Meng, Y., Pickard, C.J., Walsh, J.P.S., Rondinelli, J.M., Jacobsen, S.D., Freedman, D.E.: Computationally Directed Discovery of MoBi₂. *J. Am. Chem. Soc.* **143**, 214–222 (2021)
- [187] Pauling, L.: *The Nature of the Chemical Bond* vol. 260. Cornell University Press, Ithaca, NY (1960)

- [188] Goncharov, A.F., Struzhkin, V.V., Somayazulu, M.S., Hemley, R.J., Mao, H.K.: Compression of ice to 210 gigapascals: Infrared evidence for a symmetric hydrogen-bonded phase. *Science* **273**(5272), 218–220 (1996)
- [189] Bernasconi, M., Silvestrelli, P., Parrinello, M.: *Ab initio* infrared absorption study of the hydrogen-bond symmetrization in ice. *Phys. Rev. Lett.* **81**(6), 1235 (1998)
- [190] Zhang, L., Wang, Y., Zhang, X., Ma, Y.: High-pressure phase transitions of solid HF, HCl, and HBr: An *ab initio* evolutionary study. *Phys. Rev. B* **82**(1), 014108 (2010)
- [191] Errea, I., Calandra, M., Pickard, C.J., Nelson, J.R., Needs, R.J., Li, Y., Liu, H., Zhang, Y., Ma, Y., Mauri, F.: Quantum hydrogen-bond symmetrization in the superconducting hydrogen sulfide system. *Nature* **532**(7597), 81–84 (2016)
- [192] Vij, A., Pavlovich, J.G., Wilson, W.W., Vij, V., Christe, K.O.: Experimental Detection of the Pentazacyclopentadienide (Pentazolate) Anion, *cyclo-N₅⁻*. *Angew. Chem.* **114**, 3177–3180 (2002)
- [193] Wang, P., Xu, Y., Lin, Q., Lu, M.: Recent advances in the syntheses and properties of polynitrogen pentazolate anion *cyclo-N₅⁻* and its derivatives. *Chem. Soc. Rev.* **47**, 7522–7538 (2018)
- [194] Shen, Y., Oganov, A.R., Qian, G., Zhang, J., Dong, H., Zhu, Q., Zhou, Z.: Novel lithium-nitrogen compounds at ambient and high pressures. *Sci. Rep.* **5**, 14204 (2015)
- [195] Peng, F., Yao, Y., Liu, H., Ma, Y.: Crystalline LiN₅ Predicted from First-Principles as a Possible High-Energy Material. *J. Phys. Chem. Lett.* **6**, 2363–2366 (2015)
- [196] Laniel, D., Weck, G., Loubeyre, P.: Direct Reaction of Nitrogen and Lithium up to 75 GPA: Synthesis of the Li₃N, LiN, LiN₂, and LiN₅ Compounds. *Inorg. Chem.* **57**, 10685–10693 (2018)
- [197] Zhou, M., Sui, M., Shi, X., Zhao, Z., Guo, L., Liu, B., Liu, R., Wang, P., Liu, B.: Lithium Pentazolate Synthesized by Laser Heating-Compressed Lithium Azide and Nitrogen. *J. Phys. Chem. C* **124**, 11825–11830 (2020)
- [198] Laniel, D., Weck, G., Gaiffe, G., Garbarino, F., Loubeyre, P.: High-Pressure Synthesized Lithium Pentazolate Compound Metastable under Ambient Conditions. *J. Phys. Chem. Lett.* **9**, 1600–1604 (2018)
- [199] Steele, B.A., Oleynik, I.I.: Sodium pentazolate: A nitrogen rich high energy density material. *Chem. Phys. Lett.* **643**, 21–26 (2016)

- [200] Peng, F., Han, Y., Liu, H., Yao, Y.: Exotic stable cesium polynitrides at high pressure. *Sci. Rep.* **5**, 16902 (2015)
- [201] Li, J., Sun, L., Wang, X., Zhu, H., Miao, M.: Simple Route to Metal *cyclo-N₅⁻* Salt: High-Pressure Synthesis of CuN₅. *J. Phys. Chem. C* **122**, 22339–22344 (2018)
- [202] Xia, K., Zheng, X., Yuan, J., Liu, C., Gao, H., Wu, Q., Sun, J.: Pressure-Stabilized High-Energy-Density Alkaline-Earth-Metal Pentazolate Salts. *J. Phys. Chem. C* **123**, 10205–10211 (2019)
- [203] Liu, Z., Li, D., Tian, F., Duan, D., Li, H., Cui, T.: Moderate Pressure Stabilized Pentazolate Cyclo-N₅⁻ Anion in Zn(N₅)₂ Salt. *Inorg. Chem.* **59**, 8002–8012 (2020)
- [204] Huang, B., Frapper, G.: Barium-Nitrogen Phases Under Pressure: Emergence of Structural Diversity and Nitrogen-Rich Compounds. *Chem. Mater.* **30**, 7623–7636 (2018)
- [205] Wang, B., Larklimi, R., Valencia, H., Guégan, F., Frapper, G.: Prediction of Novel Tin Nitride Sn_xN_y Phases Under Pressure. *J. Phys. Chem. C* **124**, 8080–8093 (2020)
- [206] Du, X., Yao, Y., J., W., Yang, Q., Wang, G.: IrN₄ and IrN₇ as potential high-energy-density materials. *J. Chem. Phys.* **154**, 054706 (2021)
- [207] Wu, L., Tian, R., Wan, B., Liu, H., Gong, N., Chen, P., Shen, T., Yao, Y., Gou, H., Gao, F.: Prediction of Stable Iron Nitrides at Ambient and High Pressure with Progressive Formation of New Polynitrogen Species. *Chem. Mater.* **30**, 8476–8485 (2018)
- [208] Niu, S., Li, Z., Li, H., Shi, X., Yao, Z., Liu, B.: New Cadmium-Nitrogen Compounds at High Pressures. *Inorg. Chem.* **60**, 6772–6781 (2021)
- [209] Liu, L., Wang, D., Zhang, S., Zhang, H.: Pressure-stabilized GdN₆ with an armchair-antiarmchair structure as a high energy density material. *J. Mater. Chem. A* **9**, 16751–16758 (2021)
- [210] Bykov, M., Bykova, E., Ponomareva, I.A. A. V. and Abrikosov, Chariton, S., Prakapenka, V.B., Mahmood, M.F., Dubrovinsky, L., Goncharov, A.F.: Stabilization of Polynitrogen Anions in Tantalum-Nitrogen Compounds Under Pressure. *Angew. Chem.* **133**, 9085–9090 (2021)
- [211] Gao, G., Ashcroft, N.W., Miao, M., Hoffmann, R.: Novel Si Networks in the Ca/Si Phase Diagram under Pressure. *J. Phys. Chem. C* **118**, 25167–25175 (2014)

- [212] Li, W., Lu, M., Chen, L., Xin, X., Gao, L., Li, J., Zhou, X., Liu, W., Zhang, X., Zhang, M.: Crystal structures of CsSi₆ at high pressures. *Comput. Mater. Sci.* **150**, 144–148 (2018)
- [213] Hübner, J.-M., Carrillo-Cabrera, W., Prots, Y., Bobnar, M., Schwarz, U., Grin, Y.: Unconventional Metal-Framework Interaction in MgSi₅. *Angew. Chem. Int. Ed.* **58**, 12914–12918 (2019)
- [214] Zhang, S., Wang, Y., Yang, G., Ma, Y.: Silicon Framework-Based Lithium Silicides at High Pressures. *ACS Appl. Mater. Interfaces* **8**, 16761–167167 (2016)
- [215] Zurek, E., Yao, Y.: Theoretical predictions of novel superconducting phases of BaGe₃ stable at atmospheric and high pressures. *Inorg. Chem.* **54**(6), 2875–2884 (2015)
- [216] Castillo, R., Baranov, A.I., Burkhardt, U., Cardoso-Gil, R., Schnelle, W., Bobnar, M., Schwarz, U.: Germanium Dumbbells in a New Superconducting Modification of BaGe₃. *Inorg. Chem.* **55**, 4498–4503 (2016)
- [217] Hooper, J., Zurek, E.: Lithium subhydrides under pressure and their superatom-like building blocks. *ChemPlusChem* **77**, 969–972 (2012)
- [218] Schwarz, U., Wosylus, A., Rosner, H., Schnelle, W., Ormeci, A., Meier, K., Baranov, A., Nicklas, M., Leipe, S., Müller, C.J., Grin, Y.: Dumbbells of five-connected silicon atoms and superconductivity in the binary silicides MSi₃ (M = Ca, Y, Lu). *J. Am. Chem. Soc.* **134**(33), 13558–13561 (2012)
- [219] Hübner, J.-M., Akselrud, L., Schnelle, W., Burkhardt, U., Bobnar, M., Prots, Y., Grin, Y., Schwarz, U.: High-Pressure Synthesis and Chemical Bonding of Barium Trisilicide BaSi₃. *Materials* **12**, 145 (2019)
- [220] Schnelle, W., Ormeci, A., Wosylus, A., Meier, K., Grin, Y., Schwarz, U.: Dumbbells of five-connected Ge atoms and superconductivity in CaGe₃. *Inorg. Chem.* **51**(10), 5509–5511 (2012)
- [221] Nishikawa, T., Fukuoka, H., Inumaru, K.: High-Pressure Synthesis and Electronic Structure of a New Superconducting Strontium Germanide (SrGe₃) Containing Ge₂ Dumbbells. *Inorg. Chem.* **54**, 7433–7437 (2015)
- [222] Castillo, R., Schnelle, W., Baranov, A.I., Burkhardt, U., Bobnar, M., Cardoso-Gil, R., Schwarz, U., Grin, Y.: Trigermanides AEGe₃ (AE = Ca, Sr, Ba): chemical bonding and superconductivity. *Z. Naturforsch.* **71**, 585–592 (2016)

- [223] Lazicki, A., McGonegle, D., Rygg, J.R., Braun, D.G., Swift, D.C., Gorman, M.G., Smith, R.F., Heighway, P.G., Higginbotham, A., Suggit, M.J., Fratanduono, D.E., Coppari, F., Wehrenberg, C.E., Kraus, R.G., Erskine, D., Bernier, J.V., McNaney, J.M., Rudd, R.E., Collins, G.W., Eggert, J.H., Wark, J.S.: Metastability of diamond ramp-compressed to 2 terapascals. *Nature* **589**, 532–535 (2021)
- [224] Simon, A.: Metal clusters inside out. *Philos. Trans. R. Soc. A* **368**, 1285–1299 (2010)
- [225] Oka, T.: Interstellar H_3^+ . *Chem. Rev.* **113**, 8738–8761 (2013)
- [226] Wang, Z., Wang, H., Tse, J.S., Iitaka, T., Ma, Y.: Stabilization of H^{3+} in the high pressure crystalline structure of H_nCl ($n = 2-7$). *Chem. Sci.* **6**(1), 522–526 (2015)
- [227] Duan, D., Huang, X., Tian, F., Liu, Y., Li, D., Yu, H., Liu, B., Tian, W., Cui, T.: Predicted Formation of H^{3+} in Solid Halogen Polyhydrides at High Pressures. *J. Phys. Chem. A* **119**, 11059–11065 (2015)
- [228] Zeng, Q., Yu, S., Li, D., Oganov, A.R., Frapper, G.: Emergence of novel hydrogen chlorides under high pressure. *Phys. Chem. Chem. Phys.* **19**, 8236–8242 (2017)
- [229] Bi, T., Shamp, A., Terpstra, T., Hemley, R.J., Zurek, E.: The Li–F–H ternary system at high pressures. *J. Chem. Phys.* **154**(12), 124709 (2021)
- [230] Ayouz, M., Dulieu, O., Guérout, R., Robert, J., Kokoouline, V.: Potential energy and dipole moment surfaces of H_3^- molecule. *J. Chem. Phys.* **132**(19), 194309 (2010)
- [231] Hooper, J., Zurek, E.: Rubidium Polyhydrides Under Pressure: Emergence of the Linear H^{3-} Anion. *Chem. Eur. J.* **18**, 5013–5021 (2012)
- [232] Shamp, A., Hooper, J., Zurek, E.: Compressed cesium polyhydrides: Cs^+ sublattices and H^{3-} -three-connected nets. *Inorg. Chem.* **51**(17), 9333–9342 (2012)
- [233] Hooper, J., Altintas, B., Shamp, A., Zurek, E.: Polyhydrides of the alkaline earth metals: a look at the extremes under pressure. *J. Phys. Chem. C* **117**(6), 2982–2992 (2013)
- [234] Struzhkin, V.V., Kim, D.Y., Stavrou, E., Muramatsu, T., Mao, H.-k., Pickard, C.J., Needs, R.J., Prakapenka, V.B., Goncharov, A.F.: Synthesis of sodium polyhydrides at high pressures. *Nat. Commun.* **7**(1), 12267 (2016)

- [235] Liu, Y., Duan, D., Tian, F., Liu, H., Wang, C., Huang, X., Li, D., Ma, Y., Liu, B., Cui, T.: Pressure-Induced Structures and Properties in Indium Hydrides. *Inorg. Chem.* **54**, 9924–9928 (2015)
- [236] Chen, Y., Geng, H.Y., Yan, X., Sun, Y., Wu, Q., Chen, X.: Prediction of Stable Ground-State Lithium Polyhydrides under High Pressures. *Inorg. Chem.* **56**, 3867–3874 (2017)
- [237] Ye, X., Zarifi, N., Zurek, E., Hoffmann, R., Ashcroft, N.W.: High Hydrides of Scandium under Pressure: Potential Superconductors. *J. Phys. Chem. C* **122**, 6298–6309 (2018)
- [238] Xie, H., Yao, Y., Duan, D., Song, H., Zhang, Z., Jiang, S., Redfern, S.A.T., Kresin, V.Z., Pickard, C.J., Cui, T.: Hydrogen Pentagraphene-like Structure Stabilized by Hafnium: A High-Temperature Conventional Superconductor. *Phys. Rev. Lett.* **125**, 217001 (2020)
- [239] Feng, X., Zhang, J., Gao, G., Liu, H., Wang, H.: Compressed sodalite-like MgH₆ as a potential high-temperature superconductor. *RSC Adv.* **5**, 59292–59296 (2015)
- [240] Qian, S., Sheng, X., Yan, X., Chen, Y., Song, B.: Theoretical study of stability and superconductivity of ScH_n (n=4-8) at high pressure. *Phys. Rev. B* **96**, 094513 (2017)
- [241] Abe, K.: Hydrogen-rich scandium compounds at high pressures. *Phys. Rev. B* **96**, 144108 (2017)
- [242] Li, Y., Hao, J., Liu, H., Tse, J.S., Wang, Y., Ma, Y.: Pressure-stabilized Superconductive Yttrium Hydrides. *Sci. Rep.* **5**, 9948 (2015)
- [243] Zhao, J., Ao, B., Li, S., Gao, T., Ye, X.: Phase Diagram and Bonding States of Pu-H Binary Compounds at High Pressures. *J. Phys. Chem. C* **124**, 7361–7369 (2020)
- [244] Hai, Y.L., Lu, N., Tian, H.L., Jiang, M.J., Yang, W., Li, W.J., Yan, X.W., Zhang, C., Chen, X.J., Zhong, G.H.: Cage Structure and Near Room-Temperature Superconductivity in TbH_n (n = 1-12). *J. Phys. Chem. C* **125**, 3640–3649 (2021)
- [245] Semenov, D.V., Zhou, D., Kvashnin, A.G., Huang, X., Galasso, M., Kruglov, I.A., Ivanova, A.G., Gavriliuk, A.G., Chen, W., Tkachenko, N.V., Boldyrev, A.I., Troyan, I., Oganov, A.R., Cui, T.: Novel Strongly Correlated Europium Superhydrides. *J. Phys. Chem. Lett.* **12**(1), 32–40 (2021)
- [246] Sun, W., Kuang, X., Keen, H.D.J., Lu, C., Hermann, A.: Second group

- of high-pressure high-temperature lanthanide polyhydride superconductors. *Phys. Rev. B* **102**, 144524 (2020)
- [247] Abe, K.: High-pressure properties of dense metallic zirconium hydrides studied by calculations. *Phys. Rev. B* **98**, 134103 (2018)
- [248] Hooper, J., Terpstra, T., Shamp, A., Zurek, E.: The Composition and Constitution of Compressed Strontium Polyhydrides. *J. Phys. Chem. C* **118**, 6433–6447 (2014)
- [249] Wang, Y., Wang, H., Tse, J.S., Iitaka, T., Ma, Y.: Structural Morphologies of High-Pressure Polymorphs of Strontium Hydrides. *Phys. Chem. Chem. Phys.* **17**, 19379–19385 (2015)
- [250] Bi, T., Zarifi, N., Terpstra, T., Zurek, E.: The search for superconductivity in high pressure hydrides. In: Reedijk, J. (ed.) *Reference Module in Chemistry, Molecular Sciences and Chemical Engineering*, pp. 1–36. Elsevier, Waltham, MA (2019). <https://doi.org/10.1016/b978-0-12-409547-2.11435-0>
- [251] Hilleke, K.P., Zurek, E.: Rational Design of Superconducting Metal Hydrides via Chemical Pressure Tuning. *Angew. Chem. Int. Ed.* **134**, 202207589 (2022)
- [252] Shao, Z., Duan, D., Ma, Y., Yu, H., Song, H., Xie, H., Li, D., Tian, F., Liu, B., Cui, T.: Unique Phase Diagram and Superconductivity of Calcium Hydrides at High Pressures. *Inorg. Chem.* **58**, 2558–2564 (2019)
- [253] Semenov, D.V., Kvashnin, A.G., Kruglov, I.A., Oganov, A.R.: Actinium Hydrides AcH₁₀, AcH₁₂, and AcH₁₆ as High-Temperature Conventional Superconductors. *J. Phys. Chem. Lett.* **9**(8), 1920–1926 (2018)
- [254] Errea, I., Belli, F., Monacelli, L., Sanna, A., Koretsune, T., Tadano, T., Bianco, R., Calandra, M., Arita, R., Mauri, F., Flores-Livas, J.A.: Quantum crystal structure in the 250-kelvin superconducting lanthanum hydride. *Nature* **578**, 66–69 (2020)
- [255] Sun, Y., Lv, J., Xie, Y., Liu, H., Ma, Y.: Route to a superconducting phase above room temperature in electron-doped hydride compounds under high pressure. *Phys. Rev. Letters* **123**(9), 097001 (2019)
- [256] Onnes, H.K.: Further Experiments with Liquid Helium. D. On the Change of Electrical Resistance of Pure Metals at Very low Temperatures, etc. V. The Disappearance of the Resistance of Mercury,. *Proc. K. Ned. Akad. Wet. B* **14**, 113–115 (1911)

- [257] Matthias, B.T., Geballe, T.H., Geller, S., Corenzwit, E.: Superconductivity of Nb₃Sn. *Phys. Rev.* **95**, 1435 (1954)
- [258] Gavalier, J.R.: Superconductivity in Nb-Ge films above 22 K. *Appl. Phys. Lett.* **23**, 480 (1973)
- [259] Anderson, P.W., Matthias, B.T.: Superconductivity. *Science* **144**, 373–381 (1964)
- [260] Wu, M.K., Ashburn, J.R., Torng, C.J., Hor, P.H., Meng, R.L., Gao, L., Huang, Z.J., Wang, Y.Q., Chu, C.W.: Superconductivity at 93 K in a new mixed-phase Y-Ba-Cu-O compound system at ambient pressure. *Phys. Rev. Lett.* **58**, 908 (1987)
- [261] Gao, L., Xue, Y.Y., Chen, F., Xiong, Q., Meng, R.L., Ramirez, D., Chu, C.W., Eggert, J.R., Mao, H.K.: Superconductivity up to 164 K in HgBa₂Ca_{*m*-1}Cu_{*m*}O_{2*m*+2+ δ} (*m*=1,2, and 3) under quasihydrostatic pressures. *Phys. Rev. B* **50**, 4260–4263 (1994)
- [262] Finnemore, D.K., Stromberg, T.F., Swenson, C.A.: Superconducting Properties of High-Purity Niobium. *Phys. Rev.* **149**, 231–243 (1966)
- [263] Nagamatsu, J., Nakagawa, N., Muranaka, T., Zenitani, Y., Akimitsu, J.: Superconductivity at 39 K in magnesium diboride. *Nature* **410**, 63–64 (2001)
- [264] Sakata, M., Nakamoto, Y., Shimizu, K.: Superconducting state of Ca-VII below a critical temperature of 29 K at a pressure of 216 GPa. *Phys. Rev. B* **83**, 220512 (2011)
- [265] Drozdov, A.P., Eremets, M.I., Troyan, I.A.: Superconductivity above 100 K in PH₃ at high pressures (2015) [arXiv:1508.06224](https://arxiv.org/abs/1508.06224) [cond-mat.supr-con]
- [266] Drozdov, A.P., Eremets, M.I., Troyan, I.A., Ksenofontov, V., Shylin, S.I.: Conventional superconductivity at 203 Kelvin at high pressures in the sulfur hydride system. *Nature* **525**, 73–76 (2015)
- [267] Salke, N.P., Esfahani, M.M.D., Zhang, Y., Kruglov, I.A., Zhou, J., Wang, Y., Greenberg, E., Prakapenka, V.B., Liu, J., Oganov, A.R., Lin, J.-F.: Synthesis of clathrate cerium superhydride CeH₉ at 80-100 GPa with atomic hydrogen sublattice. *Nature Commun.* **10**, 4453 (2019)
- [268] Snider, E., Dasenbrock-Gammon, N., McBride, R., Debessai, M., Vindana, H., Vencatasamy, K., Lawler, K.V., Salamat, A., Dias, R.P.: Room-temperature superconductivity in a carbonaceous sulfur hydride. *Nature* **586**(7829), 373–377 (2020)

- [269] Di Cataldo, S., Heil, C., von der Linden, W., Boeri, L.: LaBH₈: Towards high- T_c low-pressure superconductivity in ternary superhydrides. *Phys. Rev. B* **104**, 020511 (2021)
- [270] Gao, M., Yan, X.-Y., Lu, Z.-Y., Xiang, T.: Phonon-mediated high-temperature superconductivity in the ternary borohydride KB₂H₈ under pressure near 12 GPa. *Phys. Rev. B* **104**, 100504 (2021)
- [271] Zhang, Z., Cui, T., Hutcheon, M.J., Shipley, A.M., Song, H., Du, M., Kresin, V.Z., Duan, D., Pickard, C.J., Yao, Y.: Design Principles for High-Temperature Superconductors with Hydrogen-Based Alloy Backbone at Moderate Pressure. *Phys. Rev. Lett.* **128**, 047001 (2022)
- [272] Matthias, B.T.: Progress in Low Temperature Physics. In: *Superconductivity in the Periodic System*, pp. 138–150. Elsevier, Amsterdam (1957)
- [273] Bardeen, J., Cooper, L.N., Schrieffer, J.R.: Microscopic Theory of Superconductivity. *Phys. Rev.* **106**, 162–164 (1957)
- [274] Bardeen, J., Cooper, L.N., Schrieffer, J.R.: Theory of Superconductivity. *Phys. Rev.* **108**, 1175–1204 (1957)
- [275] Pickett, W.E.: The next breakthrough in phonon-mediated superconductivity. *Physica C* **468**, 126–135 (2008)
- [276] Swift, R.M., White, D.: Low Temperature Heat Capacities of Magnesium Diboride (MgB₂) and Magnesium Tetraboride (MgB₄). *J. Am. Chem. Soc.* **79**, 3641–3644 (1957)
- [277] McMillan, W.L.: Transition Temperature of Strong-Coupled Superconductors. *Phys. Rev.* **167**, 331–344 (1968)
- [278] Dynes, R.C.: McMillan’s Equation and the T_c of Superconductors. *Solid State Commun.* **10**, 615–618 (1972)
- [279] Allen, P.B., Dynes, R.C.: Transition Temperature of Strong-Coupled Superconductors Reanalyzed. *Phys. Rev. B* **12**, 905–922 (1975)
- [280] Hopfield, J.J.: Angular Momentum and Transition-Metal Superconductivity. *Phys. Rev.* **186**, 443–451 (1969)
- [281] Quan, Y., Ghosh, S.S., Pickett, W.E.: Compressed hydrides as metallic hydrogen superconductors. *Phys. Rev. B* **100**, 184505 (2019)
- [282] Buzea, C., Robbie, K.: Assembling the puzzle of superconducting elements: a review. *Supercond. Sci. Technol.* **18**(1), 1 (2004)

- [283] Schilling, J.S.: Superconductivity in the alkali metals. *High Press. Res.* **26**, 145–163 (2006)
- [284] Hamlin, J.J.: Superconductivity in the metallic elements at high pressures. *Physica C* **514**, 59–76 (2015)
- [285] Shimizu, K.: Superconductivity from insulating elements under high pressure. *Physica C* **514**, 46–49 (2015)
- [286] Tuoriniemi, J., Juntunen-Nurmilaukas, K., Uusvuori, J., Pentti, E., Salmela, A., Sebedash, A.: Superconductivity in lithium below 0.4 millikelvin at ambient pressure. *Nature* **447**, 187–189 (2007)
- [287] Falge Jr., R.L.: Superconductivity of hexagonal beryllium. *Phys. Lett. A* **24**, 579–580 (1967)
- [288] Sizoo, G.J., Onnes, H.K.: Further experiments with liquid helium. Influence of elastic deformation on the supraconductivity of tin and indium. *Commun. Phys. Lab. Univ. Leiden.* **180b**, 13–26 (1925)
- [289] Jennings, L.D., Swenson, C.A.: Effects of Pressure on the Superconducting Transition Temperatures of Sn, In, Ta, Tl, and Hg. *Phys. Rev.* **112**, 31–43 (1958)
- [290] Smith, T.F., Chu, C.W.: Will Pressure Destroy Superconductivity? *Phys. Rev.* **159**, 353–359 (1967)
- [291] Struzhkin, V.V., Eremets, M.I., Gan, W., Mao, H.-k., Hemley, R.J.: Superconductivity in Dense Lithium. *Science* **298**, 1213–1215 (2002)
- [292] Shimizu, K., Ishikawa, H., Takao, D., Yagi, T., Amaya, K.: Superconductivity in compressed lithium at 20 K. *Nature* **419**, 597–599 (2002)
- [293] Deemyad, S., Schilling, J.S.: Superconducting Phase Diagram of Li Metal in Nearly Hydrostatic Pressures up to 67 GPa. *Phys. Rev. Lett.* **91**, 167001 (2003)
- [294] Chen, X.-J.: Exploring high-temperature superconductivity in hard matter close to structural instability. *Matter Radiat. Extremes* **5**, 068102 (2020)
- [295] Kasinathan, D., Kuneš, J., Lazicki, A., Rosner, H., Yoo, C.S., Scalettar, R.T., Pickett, W.E.: Superconductivity and Lattice Instability in Compressed Lithium from Fermi Surface Hot Spots. *Phys. Rev. Lett* **96**, 047004 (2006)

- [296] Profeta, G., Franchini, C., Lathiotakis, N.N., Floris, A., Sanna, A., Marques, M.A.L., Lüders, M., Massidda, S., Gross, E.K.U., Continenza, A.: Superconductivity in Lithium, Potassium, and Aluminum under Extreme Pressure: A First-Principles Study. *Phys. Rev. Lett.* **96**, 047003 (2006)
- [297] Rodriguez-Prieto, A., Bergara, A., Silkin, V.M., Echenique, P.M.: Complexity and Fermi surface deformation in compressed lithium. *Phys. Rev. B* **74**, 172104 (2006)
- [298] Xie, Y., Tse, J.S., Cui, T., Oganov, A.R., He, Z., Ma, Y., Zou, G.: Electronic and phonon instabilities in face-centered-cubic alkali metals under pressure using *ab initio* calculations. *Phys. Rev. B* **75**, 064102 (2007)
- [299] Yao, Y., Tse, J.S., Tanaka, K., Marsiglio, F., Ma, Y.: Superconductivity in lithium under high pressure investigated with density functional and Eliashberg theory. *Phys. Rev. B* **79**, 054524 (2009)
- [300] Bazhironov, T., Noffsinger, J., Cohen, M.L.: Superconductivity and electron-phonon coupling in lithium at high pressures. *Phys. Rev. B* **82**, 184509 (2010)
- [301] Rousseau, B., Xie, Y., Ma, Y., Bergara, A.: Exotic high pressure behavior of light alkali metals, lithium and sodium. *Eur. Phys. J. B* **81**, 1 (2011)
- [302] Yue, S.-Y., Cheng, L., Liao, B., Hu, M.: Electron-phonon interaction and superconductivity in the high-pressure *cI16* phase of lithium from first principles. *Phys. Chem. Chem. Phys.* **20**, 27125–27130 (2018)
- [303] Matsuoka, T., Sakata, M., Nakamoto, Y., Takahama, K., Ichimaru, K., Mukai, K., Ohta, K., Hirao, N., Ohishi, Y., Shimizu, K.: Pressure-induced reentrant metallic phase in lithium. *Phys. Rev. B* **89**, 144103 (2014)
- [304] Yan, Y., Zhang, Y., Wang, Y., Yang, G.: Pressure-induced reappearance of superconductivity in the *oC24* phase of lithium. *Solid State Commun.* **225**, 7–11 (2016)
- [305] Wittig, J.: Pressure-Induced Superconductivity in Cesium and Yttrium. *Phys. Rev. Lett.* **24**, 812–815 (1970)
- [306] Schwarz, U., Takemura, K., Hanfland, M., Syassen, K.: Crystal Structure of Cesium-V. *Phys. Rev. Lett.* **81**, 2711–2714 (1998)
- [307] Deng, Y., Schilling, J.S.: Evidence for superconductivity in Rb metal above 55 GPa pressure. *Phys. Rev. B* **100**, 041109 (2019)

- [308] Debessai, M., Hamlin, J.J., Schilling, J.S.: Comparison of the pressure dependences of T_c in the trivalent d -electron superconductors Sc, Y, La, and Lu up to megabar pressures. *Phys. Rev. B* **78**, 064519 (2008)
- [309] Slocombe, D.R., Kuznetsov, V.L., Grochala, W., Williams, R.J.P., Edwards, P.P.: Superconductivity in transition metals. *Phil. Trans. R. Soc. A* **373**, 20140476 (2015)
- [310] Ginzburg, V.L.: What problems of physics and astrophysics seem now to be especially important and interesting (thirty years later, already on the verge of XXI century)? *Phys.-Usp.* **42**, 353–373 (1999)
- [311] Ginzburg, V.L.: Nobel Lecture: On Superconductivity and Superfluidity. <https://www.nobelprize.org/uploads/2018/06/ginzburg-lecture.pdf>. Accessed: 2022-03-23 (2003)
- [312] Wigner, E., Huntington, H.B.: On the Possibility of a Metallic Modification of Hydrogen. *J. Chem. Phys.* **3**, 764–770 (1935)
- [313] Ashcroft, N.W.: Metallic Hydrogen: A High-Temperature Superconductor? *Phys. Rev. Lett.* **21**, 1748–1749 (1968)
- [314] Dias, R.P., Silvera, I.F.: Observation of the Wigner-Huntington transition to metallic hydrogen. *Science* **355**, 715–718 (2017)
- [315] Eremets, M.I., Drozdov, A.P., Kong, P.P., Wang, H.: Semimetallic molecular hydrogen at pressure above 350 GPa. *Nat. Phys.* **15**, 1246–1249 (2019)
- [316] Loubeyre, P., Occelli, F., Dumas, P.: Synchrotron infrared spectroscopic evidence of the probable transition to metal hydrogen. *Nature* **577**, 631–635 (2020)
- [317] Liu, X.-D., Dalladay-Simpson, P., Howie, R.T., Li, B., Gregoryanz, E.: Comment on "Observation of the Wigner-Huntington transition to metallic hydrogen". *Science* **357**, 2286 (2017)
- [318] Goncharov, A.F., Struzhkin, V.V.: Comment on "Observation of the Wigner-Huntington transition to metallic hydrogen". *Science* **357**, 9736 (2017)
- [319] Gregoryanz, E., Cheng, J., Dalladay-Simpson, P., Li, B., Howie, R.T., Mao, H.-K.: Everything you always wanted to know about metallic hydrogen but were afraid to ask. *Matter Radiat. Extremes* **5**, 038101 (2020)

- [320] Monacelli, L., Errea, I., Calendra, M., Mauri, F.: Black metal hydrogen above 360 GPa driven by proton fluctuations. *Nature Phys.* **17**, 63 (2021)
- [321] McMahon, J.M., Ceperley, D.M.: High-temperature superconductivity in atomic metallic hydrogen. *Phys. Rev. B* **84**, 144515 (2011)
- [322] Ashcroft, N.W.: Hydrogen Dominant Metallic Alloys: High Temperature Superconductors? *Phys. Rev. Lett.* **92**, 187002 (2004)
- [323] Smithson, H., Marianetti, C.A., Morgan, D., Van der Ven, A., Predith, A., Ceder, G.: First-principles study of the stability and electronic structure of metal hydrides. *Phys. Rev. B* **66**, 144107 (2002)
- [324] Bourgeois, N., Crivello, J.-C., Cenedese, P., Joubert, J.-M.: Systematic First-Principles Study of Binary Metal Hydrides. *ACS Comb. Sci.* **19**, 512–523 (2017)
- [325] Troyan, I.A., Semenov, D.V., Kvashnin, A.G., Sadakov, A.V., Sobolevskiy, O.A., Pudalov, V.M., Ivanova, A.G., Prakapenka, V.B., Greenberg, E., Gavriluk, A.G., Lyubutin, I.S., Struzhkin, V.V., Bergara, A., Errea, I., Bianco, R., Calandra, M., Mauri, F., Monacelli, L., Akashi, R., Oganov, A.R.: Anomalous high-temperature superconductivity in YH₆. *Adv. Mater.* **33**, 2006832–110 (2021)
- [326] Kong, P., Minkov, V.S., Kuzovnikov, M.A., Drozdov, A.P., Besedin, S.P., Mozaffari, S., Balicas, L., Balakirev, F.F., Prakapenka, V.B., Chariton, S., Knyazev, D.A., Greenberg, E., Eremets, M.I.: Superconductivity up to 243 K in the Yttrium-Hydrogen System under pressure. *Nature Commun.* **12**, 5075 (2021)
- [327] Jeon, H., Wang, C., Yi, S., Cho, J.-H.: Origin of enhanced chemical precompression in cerium hydride CeH₉. *Sci. Rep.* **10**, 16878 (2020)
- [328] Liang, X., Bergara, A., Wei, X., Wang, L., Sun, R., Liu, H., Hemley, R.J., Wang, L., Gao, G., Tian, Y.: Prediction of high-T_c superconductivity in ternary lanthanum borohydrides. *Phys. Rev. B* **104**, 134501 (2021)
- [329] Durajski, A.P., Szczeńniak, R.: New superconducting superhydride LaC₂H₈ at relatively low stabilization pressure. *Phys. Chem. Chem. Phys.*, 25070–25074 (2021)
- [330] Shatruk, M.: ThCr₂Si₂ structure type: The “perovskite” of intermetallics. *J. Solid State Chem.* **272**, 198–209 (2019)
- [331] Bi, T., Zurek, E.: Electronic Structure and Superconductivity of Compressed Metal Tetrahydrides. *Chem. Eur. J.* **27**(60), 14858–14870 (2021)

- [332] Mishra, A.K., Muramatsu, T., Liu, H., Geballe, Z.M., Somayazulu, M., Ahart, M., Baldini, M., Meng, Y., Zurek, E., Hemley, R.J.: New calcium hydrides with mixed atomic and molecular hydrogen. *J. Phys. Chem. C* **122**, 19370–19378 (2018)
- [333] Li, B., Miao, Z., Ti, L., Liu, S., Chen, J., Shi, J., Gregoryanz, E.: Predicted high-temperature superconductivity in cerium hydrides at high pressures. *J. Appl. Phys.* **126**, 235901 (2019)
- [334] Zhou, D., Semenov, D.V., Duan, D., Xie, H., Chen, W., Huang, X., Li, X., Liu, B., Oganov, A.R., Cui, T.: Superconducting praseodymium superhydrides. *Sci. Adv.* **6**, 6849 (2020)
- [335] Peña-Alvarez, M., Binns, J., Hermann, A., Kelsall, L.C., Dalladay-Simpson, P., Gregoryanz, E., Howie, R.T.: Praseodymium polyhydrides synthesized at high temperatures and pressures. *Phys. Rev. B* **100**, 184109 (2019)
- [336] Zhou, D., Semenov, D.V., Xie, H., Huang, X., Duan, D., Aperis, A., Oppeneer, P.M., Galasso, M., Kartsev, A.I., Kvashnin, A.G., Oganov, A.R., Cui, T.: High-Pressure Synthesis of Magnetic Neodymium Polyhydrides. *J. Am. Chem. Soc.* **142**(6), 2803–2811 (2020)
- [337] Kvashnin, A.G., Semenov, D.V., Kruglov, I.A., Wrona, I.A., Oganov, A.R.: High-Temperature Superconductivity in a Th-H System under Pressure Conditions. *ACS Appl. Mater. Interfaces* **10**, 43809–43816 (2018)
- [338] Semenov, D.V., Kvashnin, A.G., Ivanova, A.G., Svitlyk, V., Fominski, V.Y., Sadakov, A.V., Sobolevskiy, O.A., Pudalov, V.M., Troyan, I.A., Oganov, A.R.: Superconductivity at 161 K in thorium hydride ThH₁₀: Synthesis and properties. *Mater. Today* **33**, 36–44 (2020)
- [339] Hoffmann, R., Zheng, C.: Making and Breaking Bonds in the Solid State: The ThCr₂Si₂ Structure. *J. Phys. Chem.* **89**, 4175–4181 (1985)
- [340] Li, Y., Hao, J., Liu, H., Li, Y., Ma, Y.: The metallization and superconductivity of dense hydrogen sulfide. *J. Chem. Phys.* **140**(17), 174712 (2014)
- [341] Strobel, T.A., Ganesh, P., Somayazulu, M., Kent, P.R.C., Hemley, R.J.: Novel Cooperative Interactions and Structural Ordering in H₂S-H₂. *Phys. Rev. Lett.* **107**, 255503 (2011)
- [342] Duan, D., Liu, Y., Tian, F., Li, D., Huang, X., Zhao, Z., Yu, H., Liu, B., Tian, W., Cui, T.: Pressure-induced metallization of dense (H₂S)₂H₂ with high-*T_c* superconductivity. *Sci. Rep.* **4**, 6968 (2014)

- [343] Einaga, M., Sakata, M., Ishikawa, T., Shimizu, K., Erements, M.I., Drozdov, A.P., Troyan, I.A., Hirao, N., Ohishi, Y.: Crystal structure of the superconducting phase of sulfur hydride. *Nat. Phys.* **12**(9), 835–838 (2016)
- [344] Li, Y., Wang, L., Liu, H., Zhang, Y., Hao, J., Pickard, C.J., Nelson, J.R., Needs, R.J., Li, W., Huang, Y., Errea, I., Calandra, M., Mauri, F., Ma, Y.: Dissociation products and structures of solid H₂S at strong compression. *Phys. Rev. B.* **93**, 020103 (2016)
- [345] Gordon, E.E., Xu, K., Xiang, H., Bussmann-Holder, A., Kremer, R.K., Simon, A., Köhler, J., Whangbo, M.-H.: Structure and Composition of the 200 K-Superconducting Phase of H₂S at Ultrahigh Pressure: The Perovskite (SH⁻)(H₃S⁺). *Angew. Chem. Int. Ed.* **55**, 3682–3684 (2016)
- [346] Ishikawa, T., Nakanishi, A., Shimizu, K., Katayama-Yoshida, H., Oda, T., Suzuki, N.: Superconducting H₅S₂ phase in sulfur-hydrogen system under high-pressure. *Sci. Rep.* **6**, 23160 (2016)
- [347] Akashi, R., Sano, W., Arita, S. R. and Tsuneyuki: Possible “Magnéli” Phases and Self-Alloying in the Superconducting Sulfur Hydride. *Phys. Rev. Lett.* **117**, 075503 (2016)
- [348] Yao, Y., Tse, J.S.: Superconducting Hydrogen Sulfide. *Chem. Eur. J.* **24**, 1769–1778 (2018)
- [349] Laniel, D., Winkler, B., Bykova, E., Fedotenko, T., Chariton, S., Milman, V., Bykov, M., Prakapenka, V., Dubrovinsky, L., Dubrovinskaja, N.: Novel sulfur hydrides synthesized at extreme conditions. *Phys. Rev. B.* **102**, 134109 (2020)
- [350] Ortenzi, L., Cappelluti, E., Pietronero, L.: Band structure and electron-phonon coupling in H₃S: A tight-binding model. *Phys. Rev. B* **94**(6), 064507 (2016)
- [351] Durajski, A.P., Szczęśniak, R. R., Li, Y.: Non-BCS thermodynamic properties of H₂S superconductor. *Physica C* **515**, 1–6 (2015)
- [352] Durajski, A.P.: Quantitative analysis of nonadiabatic effects in dense H₃S and PH₃ superconductors. *Scientific reports* **6**(1), 1–8 (2016)
- [353] Gor'kov, L.P., Kresin, V.Z.: Pressure and high- T_c superconductivity in sulfur hydrides. *Sci. Rep.* **6**(1), 1–7 (2016)
- [354] Goncharov, A.F., Lobanov, S.S., Kruglov, I., Zhao, X.-M., Chen, X.-J., Oganov, A.R., Konôpková, Z., Prakapenka, V.B.: Hydrogen sulfide at high pressure: Change in stoichiometry. *Phys. Rev. B* **93**(17), 174105

(2016)

- [355] Jarlborg, T., Bianconi, A.: Breakdown of the Migdal approximation at Lifshitz transitions with giant zero-point motion in the H₃S superconductor. *Sci. Rep.* **6**(1), 1–12 (2016)
- [356] Bussmann-Holder, A., Köhler, J., Simon, A., Whangbo, M., Bianconi, A.: Multigap superconductivity at extremely high temperature: a model for the case of pressurized H₂S. *J. Supercond. Nov. Magn.* **30**(1), 151–156 (2017)
- [357] Szcześniak, R., Durajski, A.P.: The isotope effect in H₃S superconductor. *Solid State Commun.* **249**, 30–33 (2017)
- [358] Azadi, S., Kühne, T.D.: High-pressure hydrogen sulfide by diffusion quantum Monte Carlo. *J. Chem. Phys.* **146**(8), 084503 (2017)
- [359] Arita, R., Koretsune, T., Sakai, S., Akashi, R., Nomura, Y., Sano, W.: Nonempirical Calculation of Superconducting Transition Temperatures in Light-Element Superconductors. *Advanced Materials* **29**(25), 1602421 (2017)
- [360] Quan, Y., Pickett, W.E.: Van Hove singularities and spectral smearing in high-temperature superconducting H₃S. *Phys. Rev. B* **93**(10), 104526 (2016)
- [361] Sano, W., Koretsune, T., Tadano, T., Akashi, R., Arita, R.: Effect of Van Hove singularities on high- T_c superconductivity in H₃S. *Phys. Rev. B* **93**(9), 094525 (2016)
- [362] Heil, C., Boeri, L.: Influence of bonding on superconductivity in high-pressure hydrides. *Phys. Rev. B* **92**, 060508 (2015)
- [363] Ge, Y., Zhang, F., Yao, Y.: First-principles demonstration of superconductivity at 280 K in hydrogen sulfide with low phosphorus substitution. *Phys. Rev. B*, 224513 (2016)
- [364] Ge, Y., Zhang, F., Dias, R.P., Hemley, R.J., Yao, Y.: Hole-doped room-temperature superconductivity in H₃S_(1-x)Z_x (Z=C,Si). *Mater. Today Phys.* **15**, 100330 (2020)
- [365] Liu, B., Cui, W., Shi, J., Zhu, J., Chen, J., Lin, S., Su, R., Ma, J., Yang, K., Xu, M., Hao, J., Durajski, A.P., Qi, J., Li, Y., Li, Y.: Effect of covalent bonding on the superconducting temperature of the H-S-Se system. *Phys. Rev. B*, 174101 (2018)
- [366] Amsler, M.: Thermodynamics and superconductivity in S_xSe_{1-x}H₃.

- Phys. Rev. B **99**, 060102 (2019)
- [367] Guan, H., Sun, Y., Liu, H.: Superconductivity of H₃S doped with light elements. Phys. Rev. Res. **3**, 043102 (2021)
- [368] Wang, X., Bi, T., Hilleke, K.P., Lamichhane, A., Hemley, R.J., Zurek, E.: Dilute Carbon in H₃S Under Pressure. *npj Comput. Mater.* **8**, 87 (2022)
- [369] Cui, W., Bi, T., Shi, J., Li, Y., Liu, H., Zurek, E., Hemley, R.J.: Route to high- T_c superconductivity via CH₄-intercalated H₃S hydride perovskites. Phys. Rev. B **101**(13), 134504 (2020)
- [370] Lamichhane, A., Kumar, R., Ahart, M., Salke, N.P., Dasenbrock-Gammon, N., Snider, E., Meng, Y., Lavina, B., Chariton, S., Prakapenka, V.B., Somayazulu, M., Dias, R.P., Hemley, R.J.: X-ray diffraction and equation of state of the C-S-H room-temperature superconductor. J. Chem. Phys. **155**, 114703 (2021)
- [371] Goncharov, A.F., Bykova, E., Bykov, M., Zhang, X., Wang, Y., Chariton, S., Prakapenka, V.B., Smith, J.S.: Synthesis and structure of carbon-doped H₃S compounds at high pressure. J. Appl. Phys. **131**, 025902 (2022)
- [372] Sun, Y., Tian, Y., Jiang, B., Li, X., Li, H., Iitaka, T., Zhong, X., Xie, Y.: Computational discovery of a dynamically stable cubic SH₃-like high-temperature superconductor at 100 GPa via CH₄ intercalation. Phys. Rev. B **101**(17), 174102 (2020)
- [373] Harshman, D.R., Fiory, A.T.: The superconducting transition temperatures of C-S-H based on inter-sublattice S-H₄-tetrahedron electronic interactions. J. Appl. Phys. **131**, 015105 (2022)
- [374] Hirsch, J.E., Marsiglio, F.: Unusual width of the superconducting transition in a hydride. Nature **569**, 9–10 (2021)
- [375] Gubler, M., Flores-Livas, J.A., Kozhevnikov, A., Goedecker, S.: Missing theoretical evidence for conventional room-temperature superconductivity in low-enthalpy structures of carbonaceous sulfur hydrides. Phys. Rev. Mater. **6**, 014801 (2022)
- [376] Bykova, E., Bykov, M., Chariton, S., Prakapenka, V.B., Glazyrin, K., Aslandukov, A., Aslandukova, A., Criniti, G., Kurnosov, A., Goncharov, A.F.: Structure and composition of C-S-H compounds up to 143 GPa. Phys. Rev. B **103**, 140105 (2021)
- [377] Somayazulu, M.S., Finger, L.W., Hemley, R.J., Mao, H.K.: High-Pressure Compounds in Methane-Hydrogen Mixtures. Science **271**,

1400–1402 (1996)

- [378] Smith, G.A., Collings, I.E., Snider, E., Smith, D., Petitgirard, S., Smith, J., White, M., Jones, E., Ellison, P., Lawler, K.V., Dias, R.P., Salamat, A.: Lower pressure phases and metastable states of superconducting photo-induced carbonaceous sulfur hydride (2021) [arXiv:2111.15051](https://arxiv.org/abs/2111.15051) [cond-mat.supr-con]
- [379] Fu, Y., Du, X., Zhang, L., Peng, F., Zhang, M., Pickard, C.J., Needs, R.J., Singh, D.J., Zheng, W., Ma, Y.: High-pressure phase stability and superconductivity of pnictogen hydrides and chemical trends for compressed hydrides. *Chem. Mater.* **28**(6), 1746–1755 (2016)
- [380] Liu, H., Li, Y., Gao, G., Tse, J.S., Naumov, I.I.: Crystal structure and superconductivity of PH₃ at high pressures. *J. Phys. Chem. C* **120**(6), 3458–3461 (2016)
- [381] Shamp, A., Terpstra, T., Bi, T., Falls, Z., Avery, P., Zurek, E.: Decomposition products of phosphine under pressure: PH₂ stable and superconducting? *J. Am. Chem. Soc.* **138**(6), 1884–1892 (2016)
- [382] Flores-Livas, J.A., Amsler, M., Heil, C., Sanna, A., Boeri, L., Profeta, G., Wolverton, C., Goedecker, S., Gross, E.K.U.: Superconductivity in metastable phases of phosphorus-hydride compounds under high pressure. *Phys. Rev. B* **93**(2), 020508 (2016)
- [383] Bi, T., Miller, D.P., Shamp, A., Zurek, E.: Superconducting phases of phosphorus hydride under pressure. Stabilization by mobile molecular hydrogen. *Angew. Chem. Int. Ed.* **56**(34), 10192–10195 (2017)
- [384] Liu, M., Huang, X., Wang, X., Huang, Y., Li, F., Wu, G., Li, X., Liang, Y., Zhou, M. D. and Lu, Liu, B., Cui, T.: Unravelling decomposition products of phosphine under high pressure. *J. Raman Spectrosc.* **49**, 721–727 (2018)
- [385] Yuan, Y., Li, Y., Fang, G., Liu, G., Pei, C., Li, X., Zheng, H., Yang, K., Wang, L.: Stoichiometric evolutions of PH₃ under high pressure: implication for high- T_c superconducting hydrides. *Nat. Sci. Rev.* **6**, 524–531 (2019)
- [386] Li, X., Xie, Y., Sun, Y., Huang, P., Liu, H., C., C., Ma, Y.: Chemically Tuning Stability and Superconductivity of P-H Compounds. *J. Phys. Chem. Lett.* **11**, 935–939 (2020)
- [387] Shao, Z., Duan, D., Ma, Y., Yu, H., Song, H., Xie, H., Li, D., Tian, F., Liu, B., Cui, T.: Ternary superconducting phosphorus hydrides stabilized via lithium. *npj Comput. Mater.* **5**, 104 (2019)

- [388] Geng, N., Bi, T., Zurek, E.: Structural Diversity and Superconductivity in S-P-H Ternary Hydrides Under Pressure. *J. Phys. Chem. C* **126**, 7208–7220 (2022)